ProQuest LLC.
789 East Eisenhower Parkway
P.O. Box 1346
Ann Arbor, MI 48106 – 1346

A MÖSSBAUER STUDY OF CHROMITE-MAGNESIA REFRACTORIES

Roger Smith

A thesis submitted in partial fulfilment of the
requirements of
Sheffield Hallam University
for the degree of Master of Philosphy

JUNE 1994

Collaborating Organisation: Steetley Refractories Ltd.

A Mössbauer Study of Chromite-Magnesia Refractories

by

Roger Smith

A range of natural chrome ores, containing iron in two valence states, have been investigated using the technique of Mössbauer spectroscopy. The instrumentation reqiured to carry out the technique was studied and an additional item of equipment was designed and constructed to extend the temperature range over which the effect could be observed.

All the chrome ores yielded a complex spectra which could be attributed to a combination of octahedrally and tetrahedrally co-ordinated Fe^{2+} and Fe^{3+} quadrupole doublets. A model for fitting the spectra was devised assuming the presence of octahedrally co-ordinated Fe^{3+} and tetrahedrally co-ordinated Fe^{2+}. The inhomogeneous nature of the samples caused a broadening of the tetrahedral Fe^{2+} contribution which was fitted as a distribution of three doublets. The Mössbauer parameters obtained were compared with those of pure compounds of a similar structure.

Spectra recorded from 12K to 600K enabled effective Debye temperatures to be calculated. Second order Doppler shift (S.O.D.S.) calculations gave values for θ_D of 385K and 658K for the Fe^{2+} and Fe^{3+} contributions respectively. Absorption area data gave similar values. An examination of the temperature dependence of the quadrupole splitting of the Fe^{2+} contributions appeared to confirm the validity of the proposed fitting model. Estimations of the Fe^{2+} / Fe^{3+} ratio were made using the data obtained and yielded values of 1.6 - 3.6.

CONTENTS

1 CHROMITE-MAGNESIA REFRACTORIES

The chromite-magnesia brick normally used in the linings and roofs of basic steel furnaces consists of about 60/70% chrome ore as the coarse fraction, and 30/40% magnesia as the fine fraction, fired to a temperature above 1450°C. Since the constitutions of the various magnesites and chrome ores are very variable, it follows that the constitutions of such chromite-magnesia bricks can differ appreciably. This does not apply only to different brands, but also to different batches of the same brand. This variation in constitution is one of the chief reasons for the difference of chromite-magnesia bricks in their properties and behaviour in service. In addition to the 70/30 type of chromite-magnesia brick, a variety of types with various proportions of chrome ore to magnesia and different gradings are produced for the linings of basic electric furnaces and other purposes.

The magnesia MgO used in the brick is produced from naturally occurring magnesite $MgCO_3$ or, more usually, by a process involving the reaction of the mineral dolomite $CaMg(CO_3)_2$ with sea water.

Chrome iron ore is the only rock containing sufficient chromium which occurs in adequate deposits, being found in various parts of the world. The pure compound, ferrous chromite $FeO.Cr_2O_3$ contains 68% Cr_2O_3 but the bulk ores used in the refractory industry rarely contain more than 50% Cr_2O_3 and average about 40-50%. The chromite grains of chrome ores are mixtures of spinels $A(B_2)O_4$ in which the A atoms are considered to be Fe^{2+} and Mg^{2+} and the B atoms Cr^{3+} and Al^{3+}, with smaller amounts of Fe^{3+}. On firing in air the complex chrome spinel is oxidised, resulting in black opaque B_2O_3 (not merely Fe_2O_3, but probably a solid solution of Fe_2O_3, Cr_2O_3 and Al_2O_3) in the residual chrome grains.

Generally, chromite-magnesia refractories after firing consist of an aggregate of the two constituents, together with small amounts of original chromite crystals and un-reacted magnesia. It is likely that the thermal shock resistance of the finished brick is due to the introduction of micro-cracks in the structure of the brick, which act as inhibitors to the spread of any cracks caused by thermal shock. These micro-cracks are thought to be caused by the changes in volume associated with the change in valency of the constituent atoms, especially the iron atoms, of the chrome ore on firing. For this reason a knowledge of the Fe^{2+} / Fe^{3+} ratio could be a useful aid in the manufacture of the refractory.

As will be shown in succeeding chapters, Mössbauer spectrometry is a suitable technique for the detection of the different valence states of iron and can provide an estimation of the Fe^{2+} / Fe^{3+} ratio for chrome ores.

CHAPTER TWO

THE MÖSSBAUER EFFECT

2. THE MÖSSBAUER EFFECT

The phenomenon of resonant absorption occurs between two similar bodies, when the energy emitted by one body causes the other to resonate. This is easily observed with two tuning forks of the same frequency or, in the atomic case,when sodium vapour is seen to cast a shadow when illuminated by the light from a sodium lamp. However, there are difficulties on observing the resonant absorption of gamma radiation and this led Rudolf Mössbauer to investigate the process in 1958. This work resulted in the observation of the Mössbauer Effect.

2.1 RECOIL ENERGY LOSS

When a nucleus at rest loses energy E_0 in a transition from an excited state to a ground state by emitting a gamma ray, energy E_γ, there will be a small recoil energy loss E_r due to the finite mass, M, of the nucleus. Conservation of energy gives

$$E_0 = E_\gamma + E_r \qquad (2.1)$$

Momentum conservation requires that the momentum of the gamma photon p_γ and the momentum gained by the nucleus of the system recoiling p_n are equal in magnitude and opposite in sign

$$p_n = -p_\gamma \qquad (2.2)$$

The magnitude of the momentum of the gamma ray is given by

$$p_\gamma = \frac{E_\gamma}{C} \qquad (2.3)$$

where C is the velocity of light

Since nuclei are very heavy (when their rest energy is compared to the transition energy E_0) the nonreletavistic approximation can be used to yield the expression for the recoil energy

$$E_r = \frac{p_\gamma^2}{2M} = \frac{E_\gamma^2}{2MC^2} \qquad (2.4)$$

Because E_r is small when compared to E_0 it can be assumed that $E_\gamma = E_0$ to give

$$E_r = \frac{E_0^2}{2MC^2} \qquad (2.5)$$

If a nucleus of mass M and initially at rest absorbs a gamma photon of momentum p_γ it will recoil with this momentum. The recoil energy E_r is not then available to excite the nucleus. In order to excite a level of energy E_0 the incident gamma photon must have an energy $E_0 = E_r$. This situation is shown in figure 2.1.

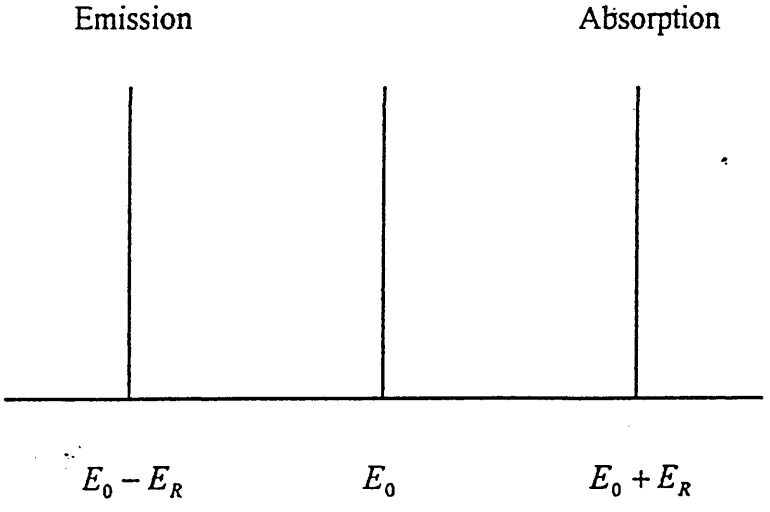

Figure 2.1 The photon emitted from a free nucleus at rest only possesses the energy $E_0 - E_r$; in order to excite the absorber it requires the energy $E_0 + E_r$

2.2 NATURAL LINE WIDTH

The energy of a state has been given as E_0 and indicated as a line. Actually these energy levels have a certain line width. The energy of the level is not "sharp" but spread over a certain energy range, as in figure 2.2.

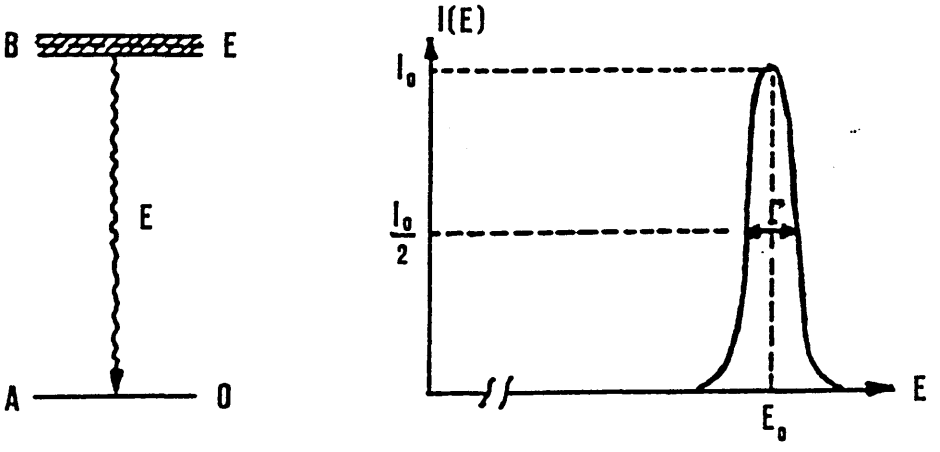

Figure 2. 2. Natural line width.

The approximate width of this range can be obtained from the uncertainty relation

$$\Delta E \Delta t \geq \hbar \qquad (2.6)$$

Here, ΔE is the uncertainty in energy and Δt the time interval available to measure the energy E. This time interval is of the order of the mean life time τ of the excited state under consideration. Setting $\Delta t \approx \tau$, gives the approximate width $\Gamma = \Delta E$ of the level

$$\Gamma = \frac{\hbar}{\tau} \qquad (2.7)$$

The ground state is stable or has a long lifetime and its energy level is well defined. The energy distribution of the emission and the absorption process is given by the Breit-Wigner formula (Breit & Wigner 1936) which can be derived classically by considering the exponentially decaying wave train with a certain amplitude. The shapes of the resulting lines are Lorentzian, with width Γ. These lines are shown in figure 2.3.

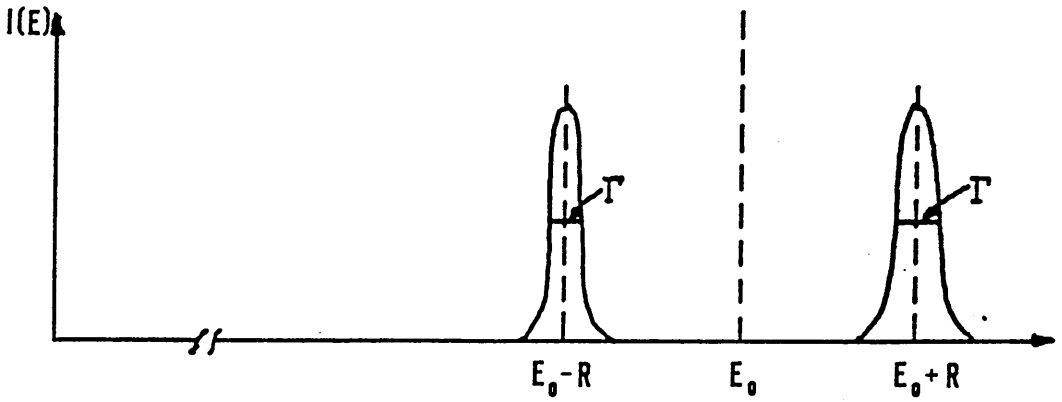

Figure 2.3. There is no overlap of emission and absorption lines even when considering the natural line width Γ.

2.3 DOPPLER BROADENING

Previously the nucleus has been considered to be free and at rest. However, in a gas or a solid, nuclei are not at rest but move with rather large velocities. In a gas the velocity can be calculated classically. The kinetic energy of a atom or molecule is given by

$$E_{kin} = \frac{1}{2} M v_0^2 = \frac{3}{2} kT \qquad (2.8)$$

Where T is the temperature (^{o}K) and k is the Boltzmann constant.

At room temperature, typical velocities are of the order of a few hundred m/sec. Such a velocity leads to a Doppler broadening.

The energy of a gamma ray emitted by a source moving with velocity component v_r along the direction of emission is shifted by an amount ΔE given by

$$\Delta E = \frac{v_r}{C} . E_0 \qquad (2.9)$$

In a gaseous source the velocity of the emitting atom will be directed at random with respect to the direction linking the source and the absorber. The velocity along the direction of emission will vary from $+v_0$ to $-v_0$ and the line shape observed from a large number of decaying atoms will be broadened by an amount

$$D \approx 2 \frac{v_0}{C} . E_0 \qquad (2.10)$$

The broadening is of the same order as E_r giving the situation illustrated in figure 2.4.

Emission and absorption lines now overlap and a small amount of resonant absorption can be expected. Unfortunately the line height is reduced by an amount Γ / D which drastically affects the number of absorbed photons. One way of increasing the amount of absorption would be to increase the temperature, so broadening the lines and increasing the overlap. However, Mössbauer observed that resonant absorption was greater at lower temperatures.

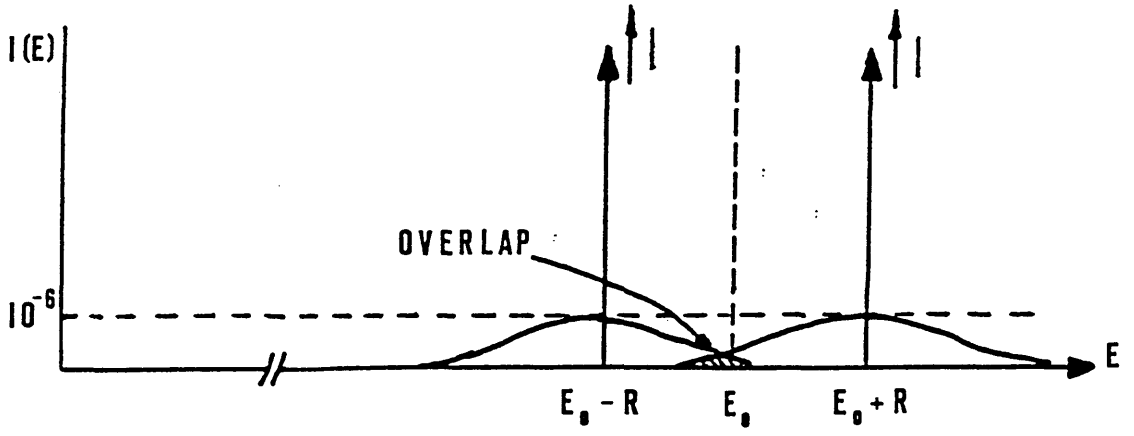

Figure 2.4. Emission and absorption lines are broadened and a small overlap exists

2.4 EINSTEIN SOLIDS

Classically, the atoms of a solid have a kinetic energy essentially in agreement with equation 2.8 and vibrate around their equilibrium positions with an energy that varies continuously with temperature. However it was suggested (Einstein 1907) that a solid is also a quantum mechanical system and that its energy should also be quantized. Assuming, for simplicity, that the energy levels of a solid should be equidistant; the energy spectrum then shows only values

$$E_g + nE_E \qquad \text{n=0,1,2,etc.}$$

In order to arrive at a crude value for the Einstein energy E_E, consider a solid with lattice constant a, and use the equation

$$E = \hbar\omega = \frac{\hbar v}{\lambda} \qquad (2.11)$$

Here, v is the velocity of the waves in the solid, and $2\pi\lambda$ is the wavelength. Assuming that $\lambda = 2a$ and taking v as the velocity of sound, gives

$$E_E = \frac{\pi\hbar v}{a} \qquad (2.12)$$

Sometimes, the Einstein temperature is given instead of the Einstein energy and it is defined by

$$\theta_E = \frac{E_E}{k} \qquad (2.13)$$

A somewhat more realistic representation of a solid, particularly at low temperatures, is the Debye model (Debye 1912). The vibrational states are given by a certain distribution of frequencies with a characteristic maximum vibrational frequency ω_D. The Debye temperature is then

$$\theta_D = \frac{\hbar\omega_D}{k} \qquad (2.14)$$

The Debye (or Einstein) temperature can be visualised as an approximate limit that separates the high temperature region where the solid can be treated in a classical fashion, from the low temperature region where quantum mechanical effects are significant.

2.5 RECOIL FREE EMISSION OF GAMMA RAYS

Now consider two different isotopes of iron whose decay schemes are given in figure 2.5.

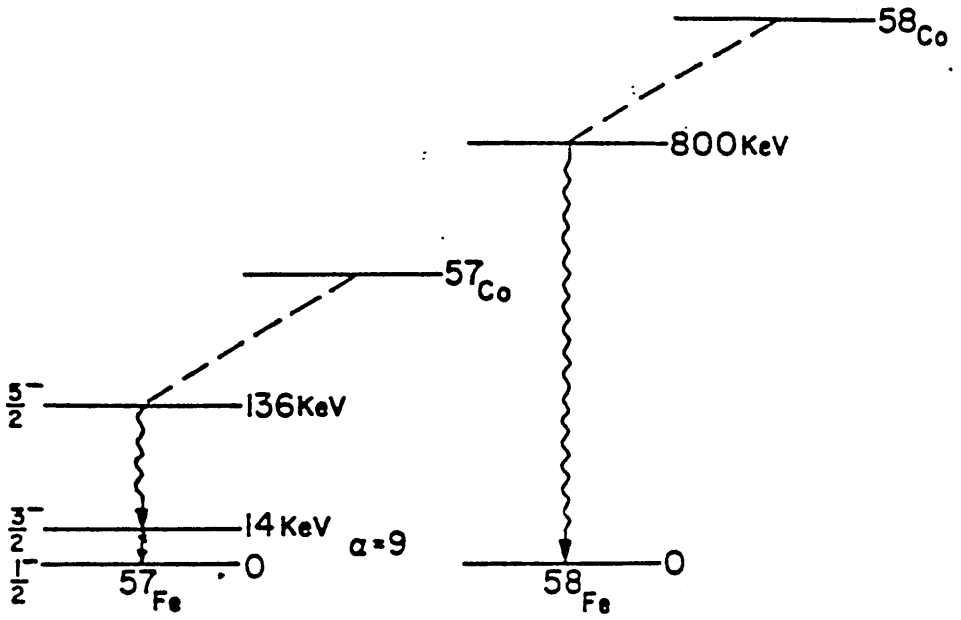

Figure 2.5 Decay schemes for ^{57}Fe and ^{58}Fe

Assuming that the decaying ^{57}Co and ^{58}Co nuclei are embedded in an-iron lattice, the following parameters for the two decay are obtained

	^{57}Fe	^{58}Fe
Decay Energy	14keV	800keV
E_R	0.002eV	6eV
E_E	0.04eV	0.04eV

For the low-energy transition the recoil energy is much smaller than the Einstein energy, whereas the opposite is true for the 800keV photons.

The minimum amount of energy that the solid can accept is E_E. Since E_R is much smaller than E_E the solid cannot accept the amount E_R and the gamma ray escapes with full energy E_0. Also, it is not Doppler broadened as the gamma ray escapes without thermal excitation of the solid and hence has the natural line shape. The situation is different for the 800keV transition. Here, E_R is very large compared to E_E and the recoil energy is absorbed giving rise to lattice vibrations and hence Doppler broadening.

Classically these are the only two possibilities, but quantum mechanically, even if E_R is much smaller than E_E there is still a small probability that the gamma ray excites the solid and leaves with less than the energy E_0. in fact, a simple calculation shows that the probability for emission with recoil energy loss is given by

$$f = e^{\frac{-E_R}{E_E}} \qquad (2.15)$$

For smaller ratios E_R / E_E a large fraction of gamma rays are emitted without Doppler broadening and without recoil energy loss.

2.6 REFERENCES

Breit G., Wigner E.

In Greenwood N.N., Gibb T.C.

'Mössbauer Spectroscopy', Chapman and Hall 1971

Debye P.P.,

In Bancoft G.M.,

'Mössbauer Spectroscopy', McGraw Hill, 1973

Einstein A.,

In Gonser U.,

'Mössbauer Spectroscopy', Springer Verlag, 1975

CHAPTER THREE

THE MÖSSBAUER SPECTROMETER

3. THE MÖSSBAUER SPECTROMETER

It has been shown in the previous chapter that it is possible to construct a source with a high proportion of recoil free emissions. However, to observe resonant absorption extra energy has to be imparted to the source.This is achieved by mechanically vibrating the source, thus varying the energy of the source via a first order Doppler effect. By controlling this motion it is possible to measure the position of the energy line in the absorber. This forms the basis of a Mössbauer spectrometer, the layout of which is shown in figure 3.1.

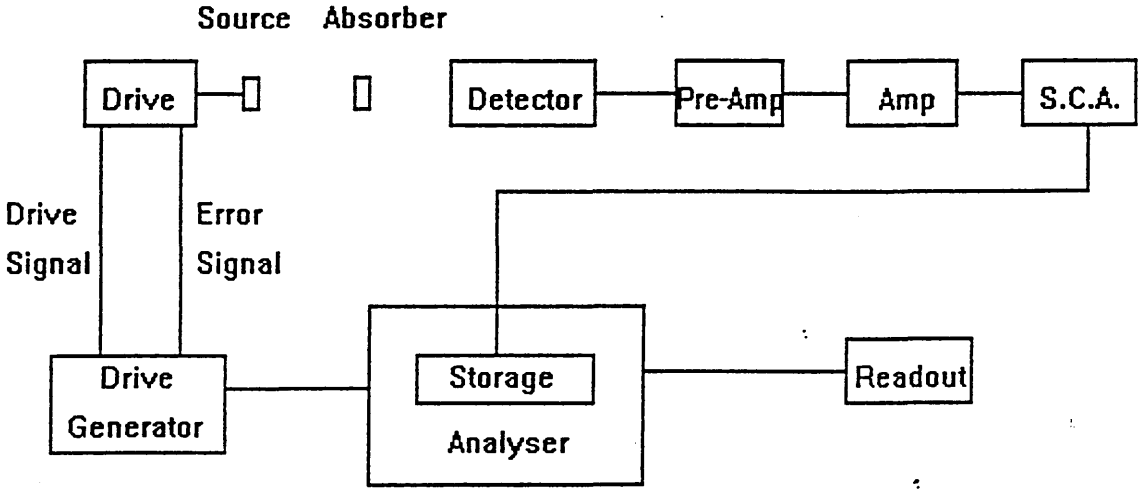

Figure 3.1 Block diagram of Mössbauer spectrometer

3.1 VELOCITY TRANSDUCER AND VELOCITY CONTROL

The Doppler velocity needed to obtain a Mössbauer spectrum is of the order of mm/sec for ^{57}Fe. This is achieved electromechanically by the use of a transducer based on the

principle of two mechanically coupled loudspeakers, as shown in figure 3.2. The driving coil causing the motion of the transducing elements and the pickup coil giving the information of the value of the velocity back to the control unit. This is used in conjunction with an analyser run in the multiscaler mode.

In the multiscaler mode the analyser accumulates counts in one channel for a specified time. Once this time has elapsed the counts accumulated are stored, the next channel is opened and the process repeated. With a large number of channels it is possible to record the variation of count rate with time. If this is repeated for each cycle of the transducer a Mössbauer spectrum can be accumulated. To synchronise the analyser with the movement of the transducer, the triangular wave form needed to drive the transducer is derived by integrating a square wave obtained from the switching of the analyser sub-groups. With an analogue to digital converter of 512 channels, the switching is set to occur at 256 and 512 channels, as shown in figure 3.3

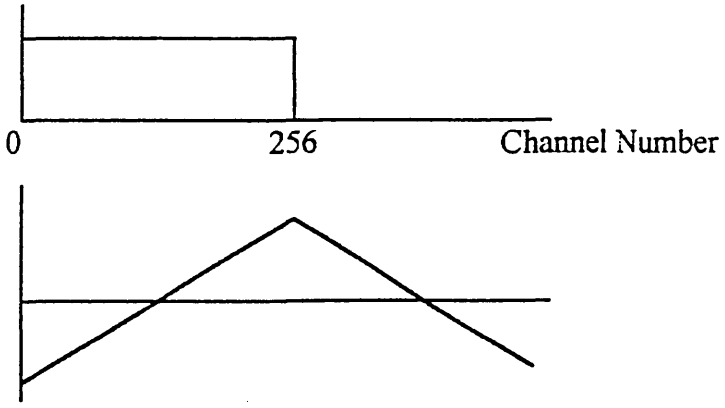

Figure 3.3 Wave forms of input voltage (top) and velocity (bottom)

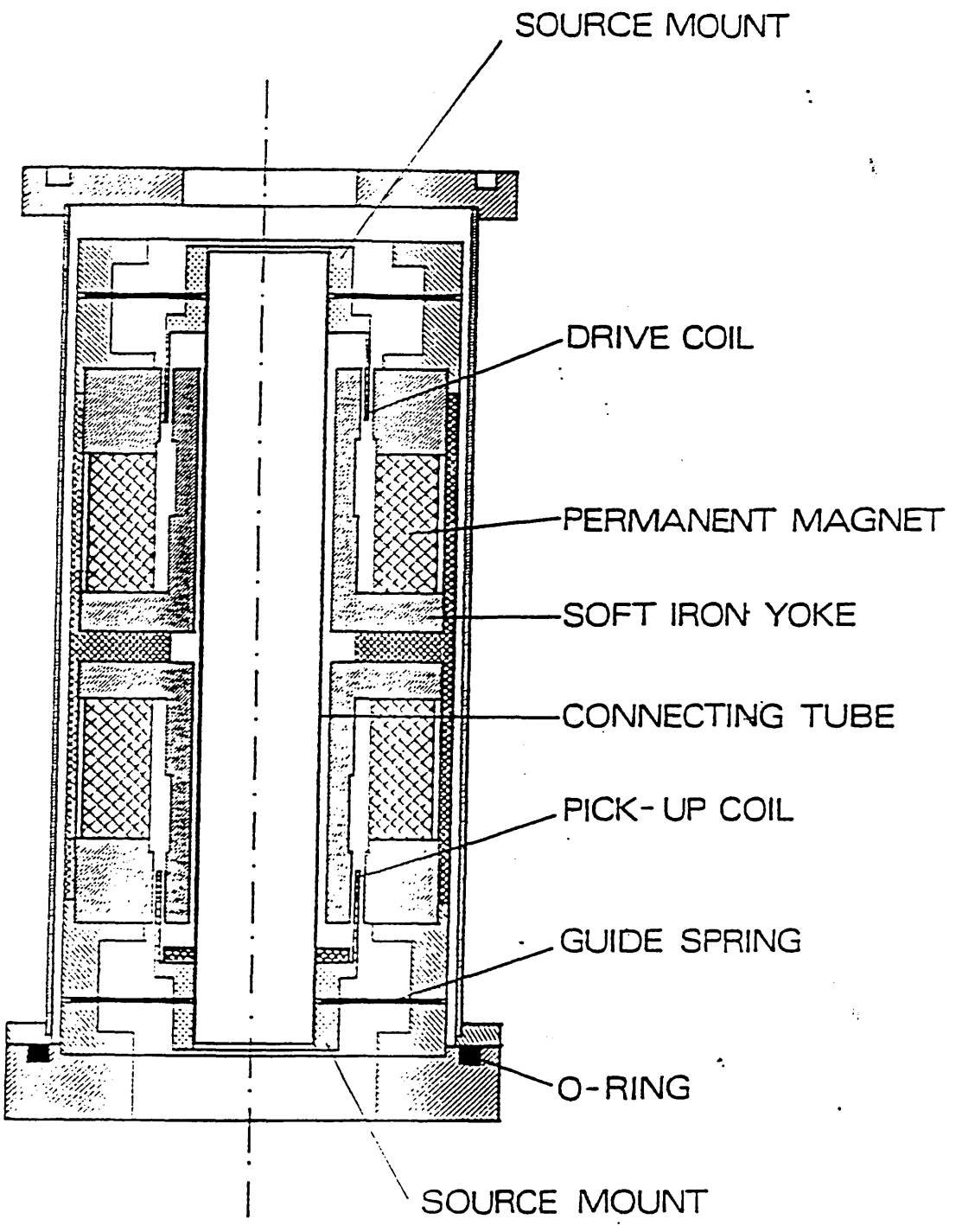

Figure 3.2 Mössbauer Velocity Transducer

The motion of the drive is a double parabola and two spectra are displayed on the multichannel analyser, one the mirror image of the other. The convention has been adopted to plot the spectrum not as a function of the Doppler energy but rather as a function of the relative velocity v . Positive velocity is usually defined as the motion of the source towards the absorber and negative velocity as the motion of the source away from the absorber.

The motion of the transducer is monitored by electronically comparing a signal derived from the pick-up coil in the transducer with the reference wave-form derived by the velocity control unit from the analyser. The drive signal is then modified to minimise any deviation from the reference wave-form. The deviation of the pick-up signal and the reference wave form is proportional to the deviation of the actual velocity from its corrected value. Using the measured error signal u_E the error of the velocity is given by

$$v_E = u_E \times calibration \cdot constant \qquad (3.1)$$

The error signal and the reference wave form are usually displayed on an oscilloscope as an indication of the correct functioning of the spectrometer.

Since the velocity tracking system controls only the transducer's velocity and not the position of the moving source mount, it is unable to prevent a slow drift of the source mount to the limit of its dynamic movement range. A position integrator has been added to the system for this purpose. The source mount's momentary position is indicated as the mean force applied by the driving coil. This mean force is proportional to the mean voltage at the output of the velocity control unit. This voltage is compared to a reference voltage v_P and additional feedback voltage supplied to re-obtain the correct mean position. The mean position can be varied by altering the reference voltage v_P.

3.2 MÖSSBAUER SOURCE

The source used in the Mössbauer spectrometers at Sheffield Hallam University is a 925 MBq (25mCi) ^{57}Co in a rhodium matrix.

Rhodium is commonly chosen as the matrix material for several reasons, it is a homogeneous alloy that is easily formed, it has good chemical stability and is non-magnetic. It has a cubic structure giving a zero electric field gradient. The recoil free fraction is high and any anomalous charge states following decay are too short lived to influence resonant nuclei.

Sources are prepared by uniformly depositing ^{57}Co onto a 6μm thick foil of rhodium. This is then diffused into the matrix at high temperatures in a controlled atmosphere to achieve dispersion. The foil is then rigidly cemented into a polyacrylate holder.

Typical properties are:-

Range of line widths, Γ_S	0.15 to 0.17 mms^{-1}
Recoilless fraction , f (At room temperature)	0.74 to 0.78

(Amersham International p.l.c.)

3.3 ABSORBERS

The absorber thickness plays a significant role in the quantitative analysis of the spectra and has been studied in detail (Williams & Brooks 1975). The effective absorber thickness, t , (for a single line absorber) is defined by

$$t = nf_a\sigma_0 \qquad (3.1)$$

where n is the number of resonant nuclei/cm^2, f_a is the recoil free fraction in the absorber and σ_0 the maximum absorption cross section. Usually experiments are carried out with a thickness of $t \sim 1$. Thicknesses greater than this produce line broadening due to saturation effects.

Absorbers are usually held in polyacrylate or high purity graphite containers. Those absorbers in powder form can be diluted with high purity graphite powder.

3.4 GAMMA RAY DETECTION

There are several types of gamma ray detectors available. Of these the gas proportional counter has a marked advantage for the detection of very low energy gamma rays. It exhibits good resolution and has a high signal to noise ratio. It's efficiency for the detection of high energy gamma rays, which are present in the decay of Mössbauer sources and contribute to the background, is negligible.

The gas proportional counter consists of a metal cylinder at ground potential with a central co-axial electrode held at a high positive potential, usually of the order of a few kilovolts. The cylinder is sealed and filled with a gaseous mixture of 95% argon and 5% methane to a pressure of one atmosphere. Gamma radiation enters the cylinder through end window of aluminised Mylar™ and once inside the detector ionises the argon atoms. The region near the central electrode has, due to the geometry of the detector, a high electric field and electrons produced in this region are accelerated towards the central electrode gaining sufficient energy to give rise to further ionisation pairs. The cumulative effect of this is to build a pulse of negative charge at the central electrode. Provided that the voltage applied to the anode is not too high as to produce an avalanche effect the size of the pulse is proportional to the energy of the incident photon and so with suitable analysis of the pulses an energy spectrum of the source can

be accumulated. A typical spectrum for ^{57}Co obtained by a gas proportional counter is shown in figure 3.4.

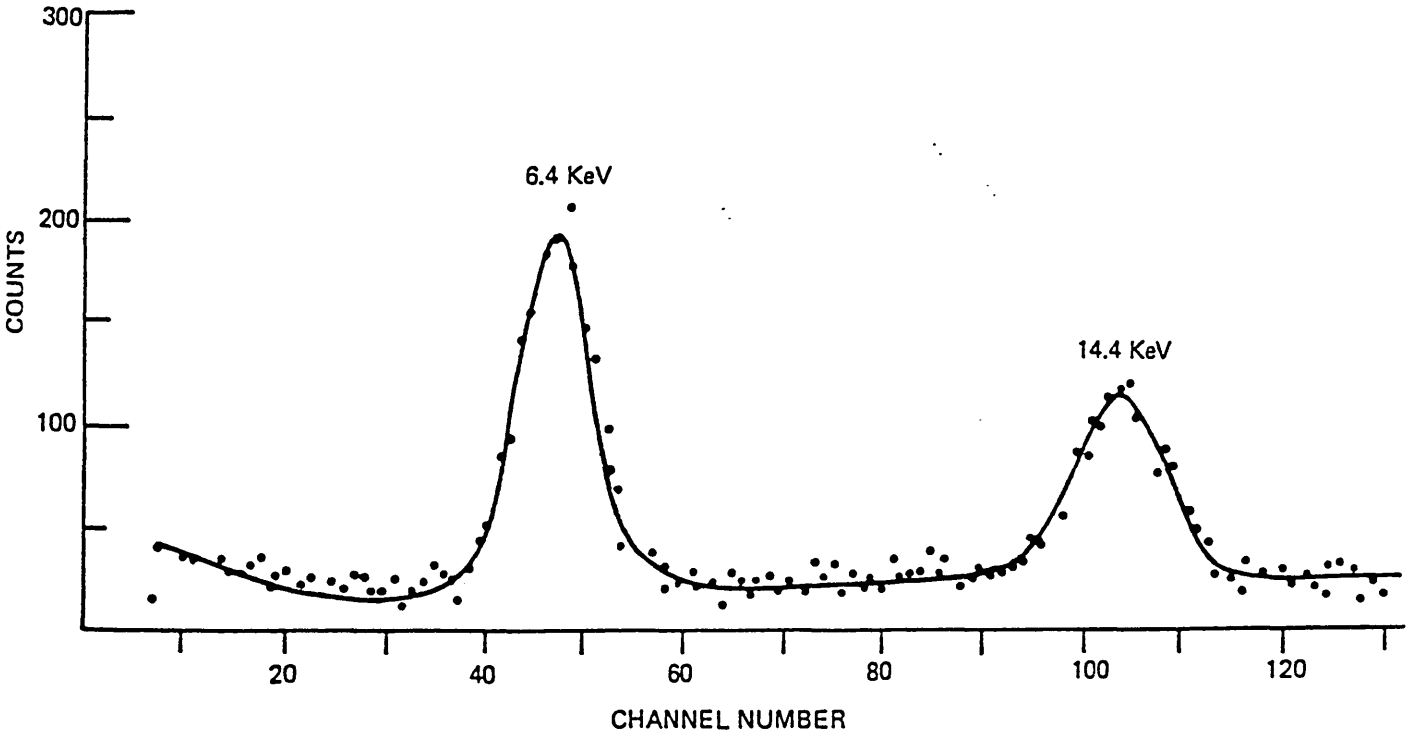

Figure 3.4 ^{57}Co spectrum from proportional counter

Argon is generally chosen as the filling gas because of its relative cheapness. However when the positively charged argon ions reach the cathode, energy is released which can eject an electron from the cathode producing a further discharge. Methane is added to the filling gas as a quench gas. Methane has a lower ionisation potential than argon and the methane molecules are ionised by the argon ions so that only methane ions reach the cathode. The energy released in this case is insufficient to release an electron from the cathode.

The voltage applied to the detector is determined by the type and pressure of the gas filling and the geometry of the detector, the geometry determining the strength of the electric field in the region of the anode. The surfaces of the electrodes need to be clean and smooth as any irregularities can affect the uniformity if the electric field. As can be seen from figure 3.5 the number of ions collected in a proportional counter is dependent upon the anode voltage and for this reason the anode voltage needs to be stable. Commercial high voltage supplies have a stability of <0.1%/h under constant load conditions.

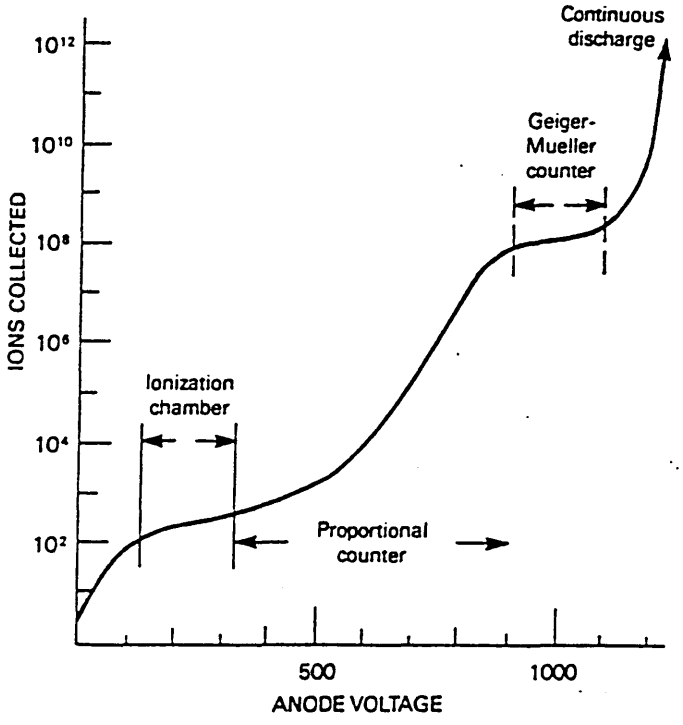

Figure 3.5 Gas detector output vs anode voltage

The pulses from the proportional counter are then amplified. Any pulses that are not attributable to the Mössbauer radiation are discriminated against by a single channel analyser before being processed by the analyser.

3.5 ANALYSIS OF DATA

The data from the accumulated Mössbauer spectra is transferred from the analyser to an Apollo 570 computer. A suite of programs have been adapted for interpretating the data (Williams 1988). The raw data is folded to reduce the mirror image spectrum to a single data set. Three programs are available for analysing the data, namely:

(1) A fitting program MOSFITN , which is essentially that written at U.K.A.E.A., Harwell, by Longworth and Cranshaw. It makes use of a non-linear least squares regression routine VA05A (G.J. Long 1984). An initial guess is made as to the Mössbauer parameters that describe the spectrum. These are then varied by the program until a best possible fit of the observed spectrum is obtained. An estimate of the goodness of fit, χ^2, is also calculated.

(2) A modified version of MOSFITN that allows data from an α-Fe or sodium nitroprusside spectrum to be analysed to calculate a calibration constant and the location of zero velocity.

(3) A distribution fitting program, PQH, based on the algorithm developed by Phillips and Twomey and applied to Mössbauer spectroscopy by Wivel and Morup (1981). It fits sums of quadrupole doublets and/or magnetic sextets to a Mössbauer spectrum.

In addition to the programs concerned with individual Mössbauer spectra, there are two further operations that deal with the parameters derived from Mössbauer spectra. Both are based on the physics of the Debye model of solids that allows estimates of the Debye temperature to be made from variation of the absorption area and the isomer shift with temperature.

3.6 CALIBRATION OF THE SPECTROMETER

As in all forms of spectroscopy, it is essential to have a method of accurately measuring the total energy scan of the source radiation and also to have a standard reference line position against which other positions may be quoted.

The six line positions from the spectrum of a natural iron foil chemically enriched with the ^{57}Fe isotope have been accurately measured and are used to measure the total velocity scan of the vibrator. The six peaks cover the range $\pm$ $5.3 mms^{-1}$. Smaller velocity scans can be calibrated by using the four inner lines of the iron spectrum.

3.7 CRYOSTATS AND FURNACES

To investigate the temperature dependent properties of absorbers the temperature of the absorber must be varied over a large range.

For the temperature range 12°K to 300°K an Air Products model DMX 20 closed cycle helium cryostat was used. This consists of a compressor stage, which produces high pressure helium to a pressure of 345 - 365 p.s.i., and an expander stage, where the expansion of the pressurised helium is controlled in a two stage refrigeration process. Figure 3.6 is a simplified diagram identifying the key elements through which the expander module produces refrigeration.

High pressure helium admitted by the rotating valve disk flows through passages in the slack cap and, at the same time, enters the regenerators,. The regenerators, cooled during the previous exhaust stroke, cool the incoming gas as it flows through. Gases flowing through the slack cap passages raise the cap to engage and lift the displacer, creating expansion space at the heat stations for the gas that has passed through the generators. Also as the displacer lifts, gas above the slack cap is partially compressed

and pushed through the orifice into the surge volume. Before the displacer reaches the valve stem, the valve closes. Compression of gas above the slack cap decelerates and stops the displacer before it can collide with the valve stem.

When the valve opens to exhaust, high pressure gas at the heat stations is free to expand and refrigerate them. The exhausting gas also cools the regenerators. As the pressure drops, partially compressed gas bleeds from the surge volume, pushes the slack cap and displacer towards the heat stations, forces exhaust, and positions the displacer for the next cycle. The valve closes again, and residual gas acts as a cushion to decelerate and stop the displacer before it collides with the heat stations. The heat station temperature is progressively reduced to provide refrigeration at cryogenic temperatures.

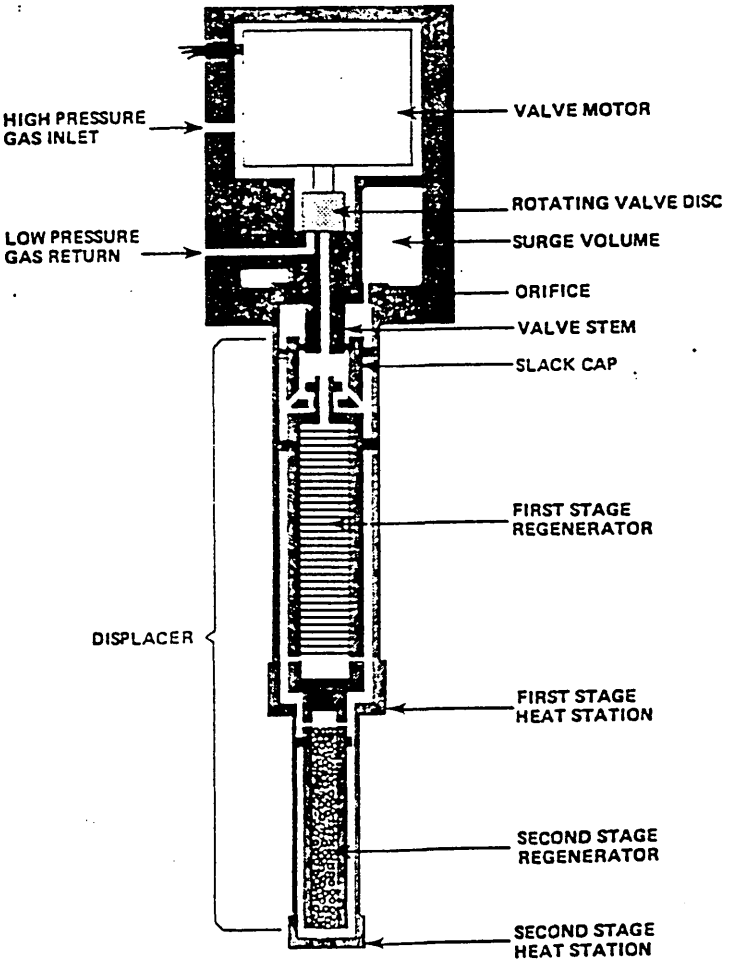

Figure 3.6 Simplified expander diagram (Air Products Ltd.)

To minimise vibrations inherent in the process, the version of the cryostat designed for Mössbauer spectroscopy isolates the sample holder from the main body of the expander module by using a heat exchanger of interleaved concentric cylinders and an exchange gas. The only physical connection between the expander module and the sample holder being convoluted rubber bellows, as shown in figure 3.7. Both parts of the system are rigidly clamped to separate structures.

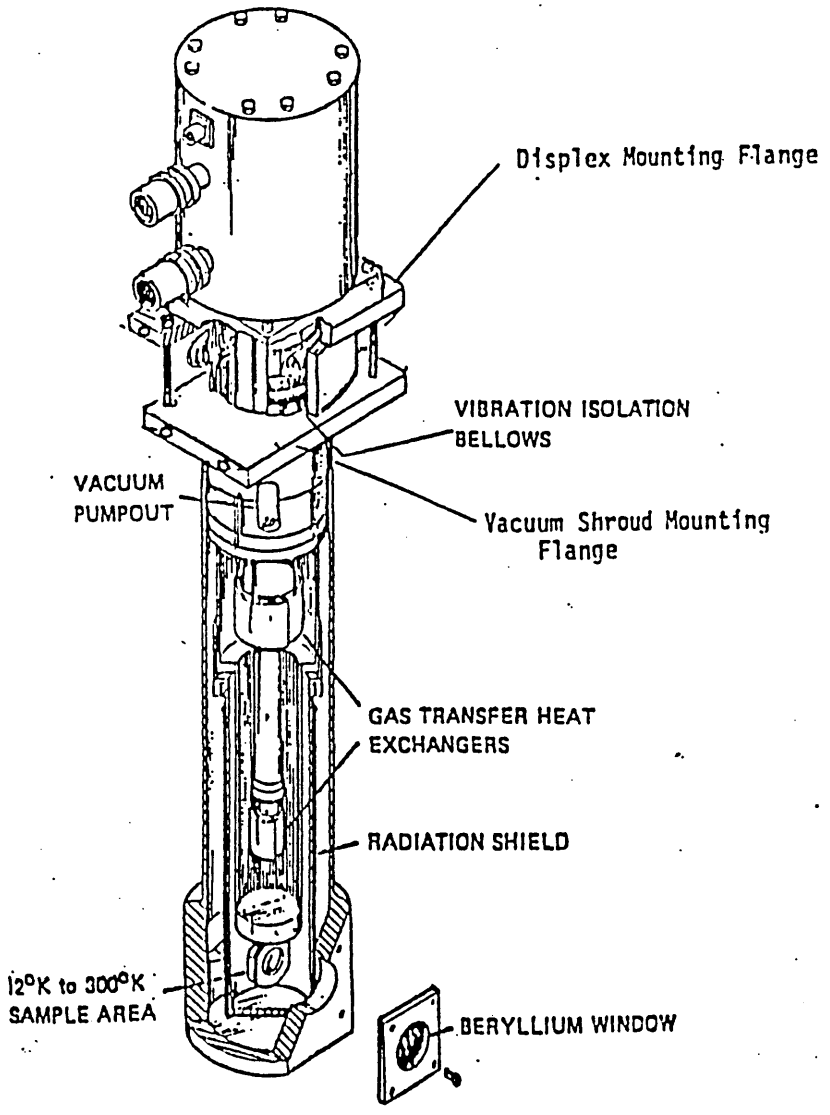

Figure 3.7 Simplified diagram of expander model DMX-20 for Mössbauer spectroscopy (Air Products Ltd.)

To cover the temperature range 300°K - 1000°K a furnace based on an initial design by Van der Woude and Boom (1965) was constructed (figure 3.8.). A Thermocoax™ insulated sheath resistance heater is wound round a former of nickel alloy and held in place by refractory cement. The nickel alloy former is supported by the main body of the furnace via a machinable ceramic ring. The conduction of heat through the stainless steel screws used as fastenings is minimised by arranging the fixing points alternately round the circumference of the ceramic ring, so that the screws fastening the heater to the ring and those fastening the ring to the body of the furnace, are separated by the maximum spacing. To reduce the amount of heat loss due to radiation a brass heat shield covers the other side of the heater. The rest of the furnace is constructed in brass and has a water cooled jacket. Entry and exit windows are of aluminised Mylar™ . The assembly is vacuum tight and is operated at approximately 10^{-2} torr.

Samples, which are held in graphite holders, are changed by removing the front plate and the heat shield giving access to the sample clamp. The sample is monitored by two type K thermocouples. One is used for temperature control and the other for temperature measurement. Temperature control is performed by an EMEC type G61 temperature controller achieving a temperature stability of ± 1°K up to 1000°K

The furnace satisfies the following design requirements

(1) The furnace is narrow, to minimise the distance between source and detector

(2) It has a large enough thermal mass to enable adequate control to 1000°K

(3) The windows are kept cool enough to maintain their integrity

(4) Easy sample changing

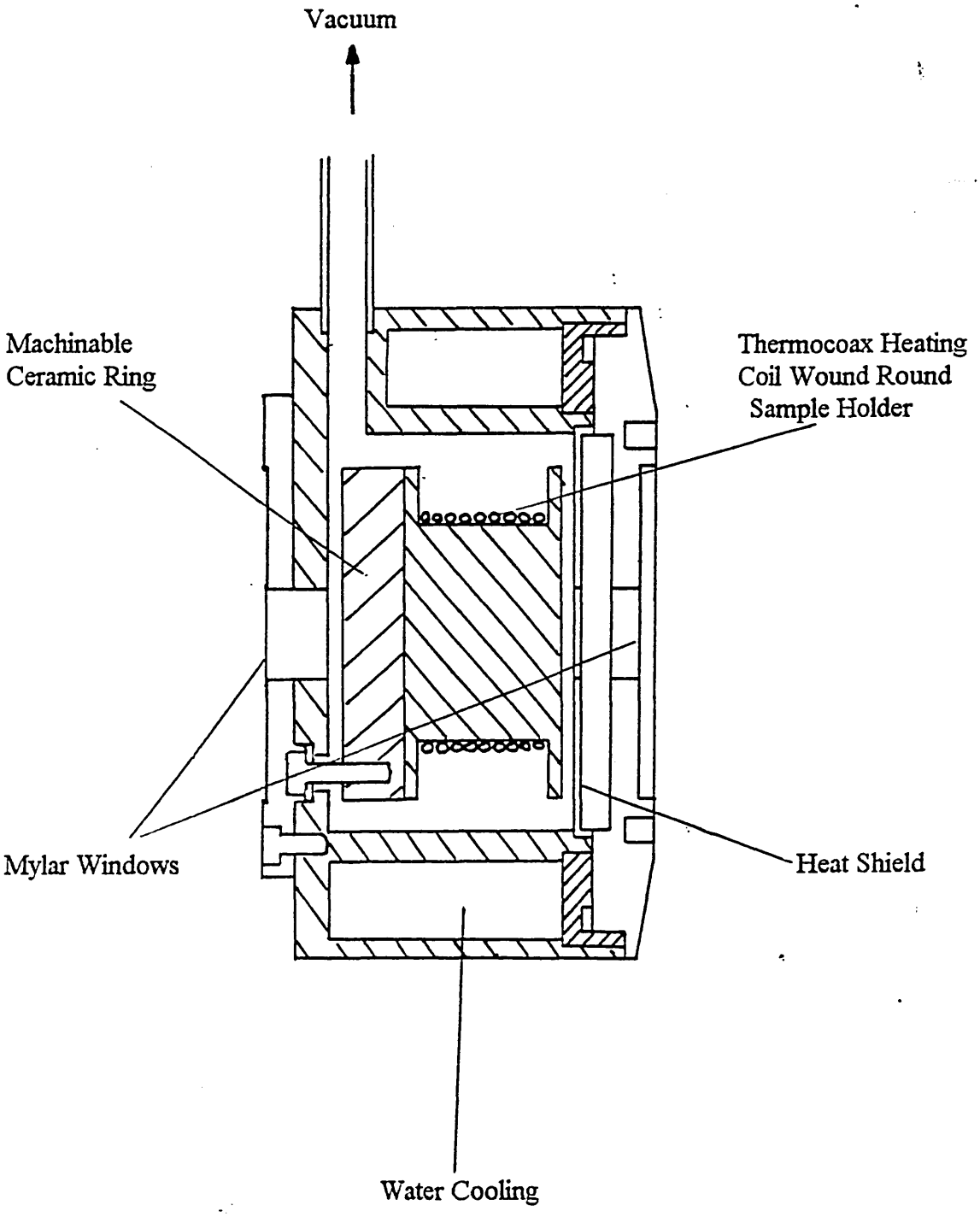

Figure 3.8 Simplified diagramn of Mössbauer furnace

3.8 REFERENCES

Long C.J., Ed.

'Mössbauer Spectroscopy Applied to Inorganic Chemistry', Chapter 4, Plenum Press, 1984

Van der Woude F., Boon G.

The Review of Scientific Instruments, 36(6), 800,1965

Williams G.W.,

'Using MOSBAR Under VM/CMS', Sheffield Hallam University Computer Services V6/3.56, 1988

Williams J.M., Brooks J.S.

Nuclear Instrumentation and Methods, 128, 363, 1975

Wivel C., Morup S.

Journal of Physics, E14, 605, 1981

CHAPTER FOUR

HYPERFINE INTERACTIONS AND MÖSSBAUER PARAMETERS

4. HYPERFINE INTERACTIONS AND MÖSSBAUER PARAMETERS

The hyperfine interactions may be regarded as those small additional interactions which occur between a nucleus and its environment as a consequence of the fact that a nucleus is not a structureless point charge, but a cluster of moving charges, distributed over a finite volume. These interactions give rise to isomer shifts δ quadrupole splittings Δ and magnetic hyperfine splittings. The Mössbauer effect affords a mechanism for measuring these small effects, and in doing so provides a highly detailed account of the way in which a nucleus interacts with its environment. (Greenwood & Gibb 1971)

4.1 ISOMER SHIFT

The mean energy of the absorbed or emitted gamma radiation is effected by the interaction of the nuclear charge distribution with the electron density at the absorbing or emitting nucleus. Assuming the nucleus is a uniformly charged sphere of radius R and that the electron charge density ρ is uniformly distributed over the nucleus, then the difference between the electrostatic interaction of a point nucleus and a nucleus with radius R is given by

$$\delta E = -\int_0^R \rho(V - V_0) 4\Pi r^2 dr \qquad (4.1)$$

where $V_0 = {}^{Z_e}/_{r}$, $V = {}^{Z_e}/_{R}\left({}^{3}/_{2} - {}^{r^2}/_{2R^2}\right)$ for r ≤ R and Z_e = nuclear charge.

This yields

$$\delta E = \frac{4\Pi\rho Ze}{R}\int_0^R\left(\frac{3}{2}-\frac{r^2}{2R^2}-\frac{R}{r}\right)r^3dr$$

$$\delta E = -\frac{2\Pi}{5}Ze\rho R^2 \qquad (4.2)$$

Taking $\rho = -e|\Psi(0)|^2$ for the electron charge density where $|\Psi(0)|^2$ is the 's' elctron charge density at the nucleus

$$\delta E = \frac{2\Pi}{5}Ze^2R^2|\Psi(0)|^2 \qquad (4.3)$$

For a transition from the excited state to the ground state

$$\delta E_\alpha - \delta E_g = \frac{2\Pi}{5}Ze^2\left(R_\alpha{}^2 - R_g{}^2\right)|\Psi(0)|^2$$

$$\delta E_\alpha - \delta E_g = \frac{2\Pi}{5}Ze^2R^2\frac{\Delta R}{R}|\Psi(0)|^2 \qquad (4.4)$$

where $\Delta R = R_\alpha - R_g$

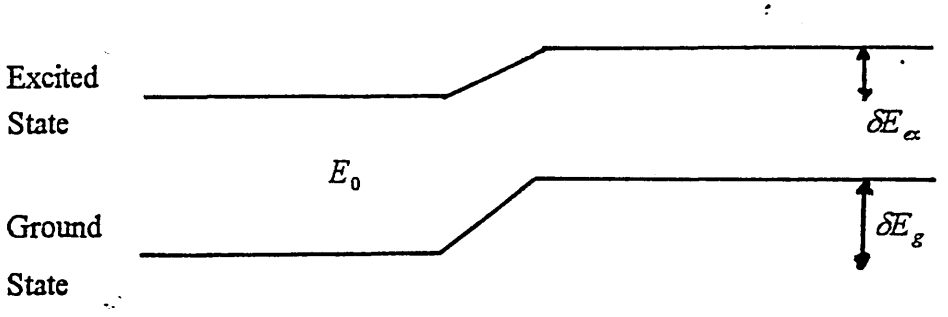

Figure 4.1 The origin of the isomer shift

Thus the shift observed in the Mössbauer effect is given by the difference between the shift in the source and the shift in the absorber, and is proportional to the difference in the electron densities at the nuclear sites in the two materials.

$$\text{Isomer Shift}\,(\delta) = \frac{2\Pi}{5} Ze^2 R^2 \frac{\Delta R}{R}\left\{\left|\Psi_{abs}(0)\right|^2 - \left|\Psi_{source}(0)\right|^2\right\} \qquad (4.5)$$

Of particular interest to this investigation is the fact that different values have been found for the isomer shift of ferrous and ferric iron. Their atomic configerations differ only by a 3d electron, which does not contribute directly to $|\Psi(0)|^2$. However, the 3d electrons screen the nuclear charge, thereby reducing the attractive coulomb potential causing the 3s electron wave function to expand, and the charge density at the nucleus to be reduced. (The 1s and 2s electrons are inside the M shell and are perturbed by the 3d electrons).

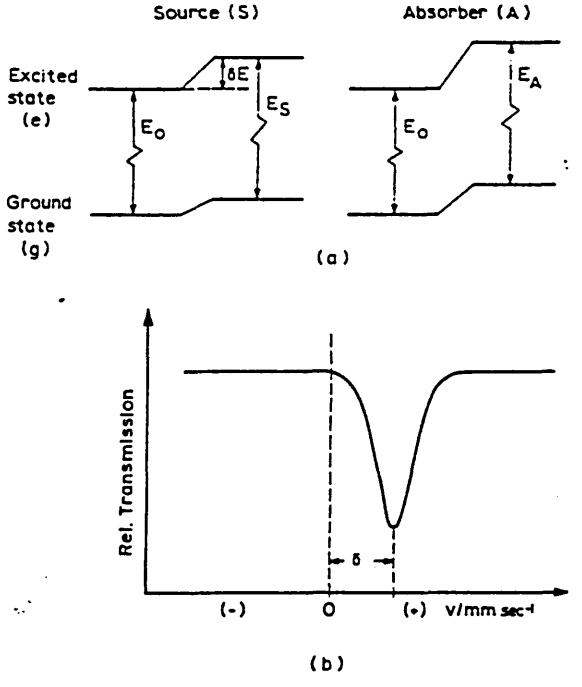

Figure 4.2 a and b. Origin of isomer shift.
(a) Electric monopole interaction shifts nuclear energy levels without lifting the degeneracy (b) resultant Mössbauer spectrum. (Greenwood & Gibb)

Thus Fe^{3+} with five 3d electrons has a larger charge density at the nucleus than Fe^{2+}.This leads to a wide seperation of the Fe^{3+} and Fe^{2+} lines in the Mössbauer spectrum (typically δ = 0.15 - 0.50 mms^{-1} for Fe^{3+}, 0.9 - 1.25 mms^{-1} for Fe^{2+} at room temperature).

We must also consider the effect of $\Delta R/R$ on the isomer shift (equation 4.5), in some cases (e.g. ^{57}Fe) this is negative which means that a positive chemical shift corresponds to a decrease in s electron density at the nucleus.

4.2 QUADRUPOLE SPLITTING

In the previous section it was assumed that the nuclear charge distribution was uniform and spherically symmetrical. In many nuclei however, the nuclear charge distribution deviates more, or less, from spherical symmetry. A measure of the deviation from spherical symmetry is given by the nuclear electric quadrupole moment Q. The sign of Q refers to the shape of the distorted nucleus: Q is negative for a flattened nucleus and positive for an elongated one. Any nuclear state with a spin I > 1/2 has a quadrupole moment and can interact with an inhomogeneous electric field described by the electric field gradient (E.F.G.) at the nucleus.

The electric field gradient at the nucleus is defined as the tensor

$$E_{ij} = -V_{ij} = -\frac{\delta^2 V}{\delta x_i x_j} \qquad (x_i x_j = x, y, z) \qquad (4.6)$$

The axis system for the electric field of the resonant atom is defined such that the maximum value of the field gradient is

$$V_{zz} = eq \qquad (4.7)$$

For each possible orientation of the nuclear spin with respect to the principal axis, Z, there will be an interaction energy between the nuclear quadrupole moment, Q, and eq. The Laplace equation requires that the electric field gradient be a traceless tensor, i.e.

$$V_{ZZ} + V_{XX} + V_{YY} = 0 \qquad (4.8)$$

This enables the electric field gradient to be defined completely by two parameters, which are usually chosen as V_{ZZ} and an asymmetry parameter η defined as

$$\eta = \frac{V_{XX} - V_{YY}}{V_{ZZ}} \qquad (4.9)$$

The components are usually chosen so that

$$|V_{ZZ}| \geq |V_{YY}| \geq |V_{XX}| \qquad (4.10)$$

making $0 \leq \eta \leq 1$

In the case of an axially symmetric field i.e. $V_{XX} = V_{YY}$ and η=0 the energy levels are given directly by (Greenwood & Gibb)

$$E_Q = \frac{e^2 qQ}{4I(2I-I)}\left[3m_I{}^2 - I(I+1)\right] \qquad (4.11)$$

where I is the spin state of the level and m_I is the magnetic quantum number.

For I = 1/2 there is only one level but for I = 3/2 there are two distinct eigen values of energy

$$E_Q\left(\pm\tfrac{3}{2}\right)=\frac{e^2qQ}{4} \qquad \text{for } m_I=\pm\tfrac{3}{2} \qquad (4.12)$$

$$E_Q\left(\pm\tfrac{1}{2}\right)=-\frac{e^2qQ}{4} \qquad \text{for } m_I=\pm\tfrac{1}{2} \qquad (4.13)$$

The difference in energy ΔE_Q between the two sub-states becomes

$$\Delta E_Q = E_Q\left(\pm\tfrac{3}{2}\right)-E_Q\left(\pm\tfrac{1}{2}\right)=\frac{e^2qQ}{2} \qquad (4.14)$$

For fields without axial symmetry the interaction Hamiltonian may only be solved exactly for a nuclei with a total spin angular momentum of I = 3/2, leading to the expression (Greenwood & Gibb)

$$E_Q=\frac{e^2qQ}{4I(2I-1)}\left[3m_I{}^2-I(I+1)\right]\left(1+\frac{\eta^2}{3}\right)^{\frac{1}{2}} \qquad (4.15)$$

The measurement of the quadrupole interaction gives the product of the nuclear moment and the EFG at the nucleus. The sources of EFG's at nuclear sites are basically of two kinds, those generated by changes in the lattice and those generated by the electronic charge cloud of the atom itself, although this distinction can often become blurred.

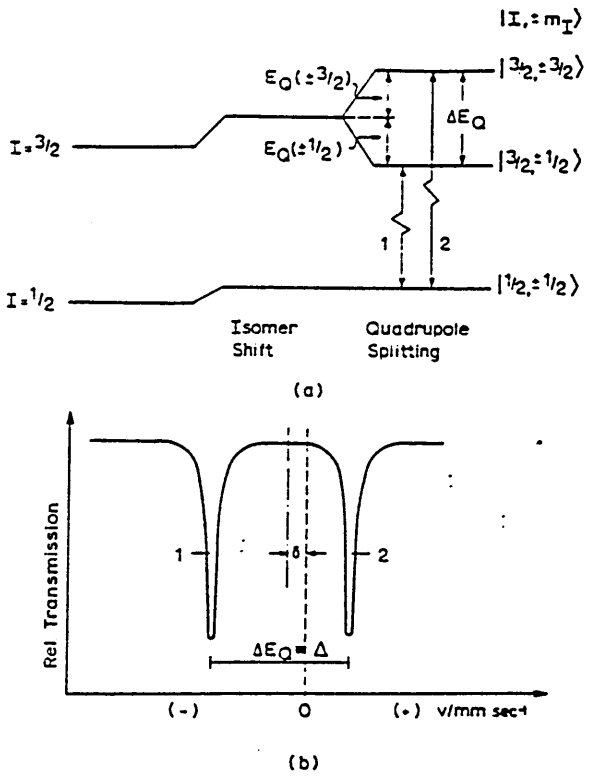

Figure 4.3 a and b. Quadrupole splitting for a nucleus with spin I = $\frac{3}{2}$ in the excited state (a) I = $\frac{3}{2}$ level is split into two sub-levels by electric quadrupole interaction (b) resultant Mössbauer spectrum (Greenwood & Gibb)

4.3 THE NUCLEAR ZEEMAN EFFECT

The interaction of the nuclear magnetic dipole moment μ with a magnetic field H at the site of the nucleus, splits the nuclear state with spin I (I>0) into 2(I+1) sub-levels with the eigen values

$$E_m = -\frac{\mu H m_I}{I} = -g_N \beta_N H m_I \qquad (4.11)$$

where m_I is the magnetic quantum number with the values m_I = I, I-1,.....-I.

The nuclear magnetic moment is related to the nuclear Bohr magneton β_N by the gyromagnetic ratio g_N

$$\mu = g_N \beta_N I \qquad (4.12)$$

The magnetic dipole splitting is shown in Fig. 4.4 for ^{57}Fe with $I_e = 3/2$ and $I_g = 1/2$. Each of the two states has a magnetic dipole moment and will therefore be split by magnetic interaction. Gamma transitions between the sub-levels of the ground state and those of the excited state are subject to selection rules. For magnetic dipole radiation (as in ^{57}Fe) only transitions with $\Delta I = 1$, $\Delta m = 0, \pm 1$ are allowed, giving six altogether in ^{57}Fe. The six transitions are shown in Fig. 4.4. Using a single line source one would expect a resonance sextet in the Mössbauer spectrum, the centroid of which may be shifted from zero velocity by an isomer shift.

It is often found that a nuclear state is simultaneously perturbed by both magnetic and electric quadrupole interactions. In this case the sub-levels of the I = 3/2 state of ^{57}Fe are no longer equally spaced, as shown in the right diagramn of Fig. 4.4

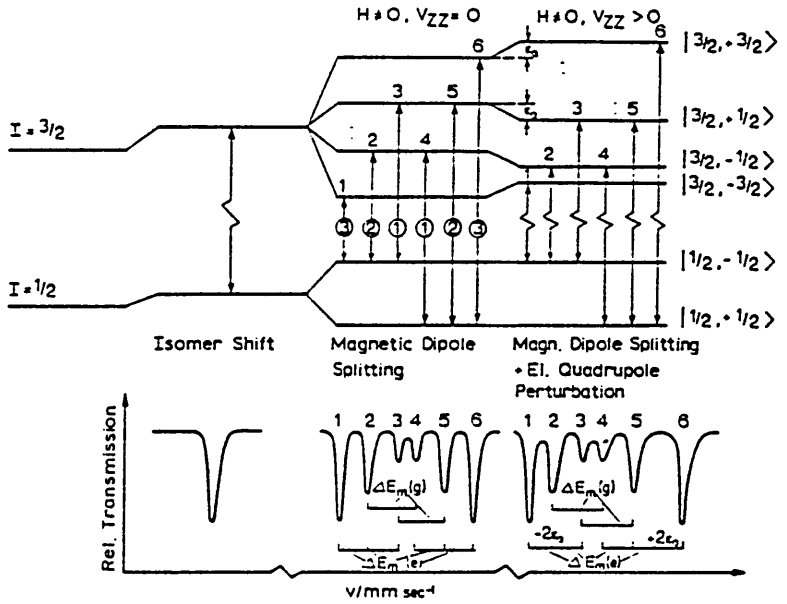

Figure 4.4 Magnetic dipole splitting with and without electric quadrupole perturbation and resultant Mössbauer spectra. (Greenwood & Gibb)

4.4 REFERENCES

General Reference

Greenwood N.N., Gibb T.C.

'Mössbauer Spectroscopy', Chapman and Hall, 1971, pp. 55-56

Bibliography

Bancroft G.M.

'Mössbauer Spectroscopy', McGraw Hill, 1973

Goldanskii V.I., Herber R.H.

'Chemical Applications of Mössbauer Spectroscopy', Academic Press, 1968

Gonser U.

'Mössbauer Spectroscopy', Springer Verlag, 1975

CHAPTER FIVE

CHROME ORES

5 CHROME ORES

Chrome ore is a basic rock containing chromite grains and the mineral serpentine, $Mg_2Si_2O_5(OH)_4$, sometimes called the 'gangue'. Natural chromites have been studied using chemical and X-ray analysis to determine their composition and cation distribution (Clark & Ally 1932, De Wet & Van Niekerk 1952, Chatraborky 1965). The chromite grains are isomorphous mixtures of spinels $A(B_2)O_4$ in which the A sites are considered to be occupied by the divalent ions Fe^{2-} and Mg^{2+}, and the B sites by the trivalent ions Cr^{3-}, Al^{3+} and Fe^{3+}. Hence the various spinels are $FeAl_2O_4$, $FeCrO_4$, $FeFe_2O_4$, $MgCr_2O_4$, $MgFe_2O_4$ and $MgAl_2O_4$. Of these, $FeFe_2O_4$ and $MgFe_2O_4$ are ferro-magnetic but it has been shown (Rait 1946) that spinels may contain appreciable amounts of ferrites in solution without exhibiting ferromagnetism.

5.1 SPINEL STRUCTURE

The idealised spinel structure is shown in figure 5.1 and consists of tetrahedral (A) sites and octahedral (B) sites in a face-centered cubic oxide lattice. Spinels have the general formula $A(B_2)O_4$ and in a normal 2,3 spinel the A sites are occupied by divalent ions and the B sites by trivalent ions. It has been shown however (Barth & Posjnak 1931) that there are two types of spinel, the normal and the inverse type, in which eight of the sixteen trivalent ions on the octahedral site are replaced by eight divalent ions with the remaining trivalent ions occupying the tetrahedral sites. The general formula now becoming $B(AB)O_4$. Intermediate distributions of ions are also known and the degree of inversion, or disorder, x is defined as the fraction of tetrahedral sites occupied by trivalent ions.

A quantitative treatment of the thermodynamics of cation distribution in simple spinels (Navrotsky & Kleppa 1967) obtained emperical site preference energies for a series of divalent and trivalent ions in the spinel structure. The results of this work are shown schematically in figure 5.2. which shows the site preference energies, determined from calorimetric enthalpy measurements, for a number of different ions.

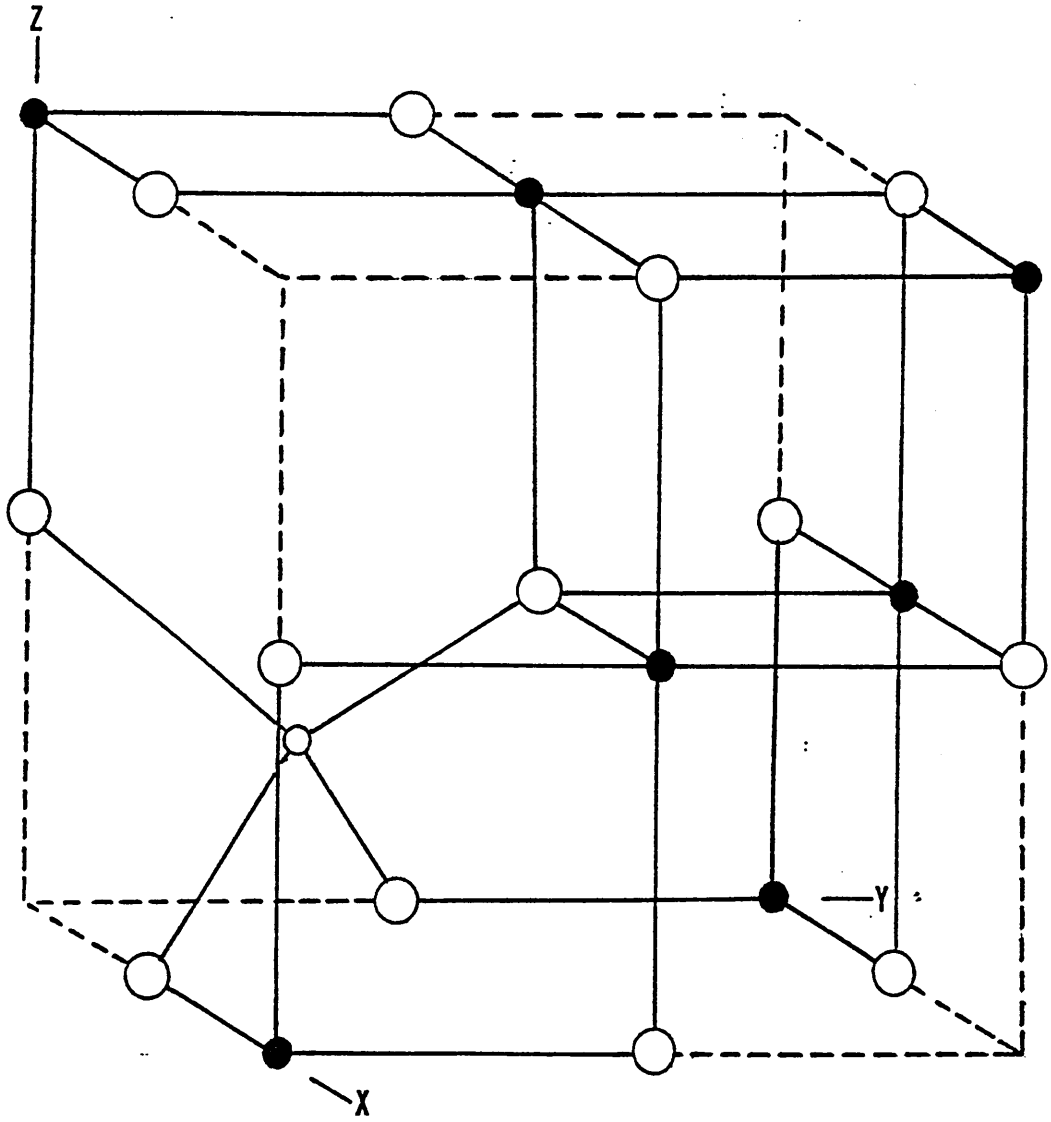

Figure 5.1 Part of the spinel crystal structure showing oxygen atoms (large circles), tetrahedral (A, small open circle) and octahedral (B, small filled circles) cation sites

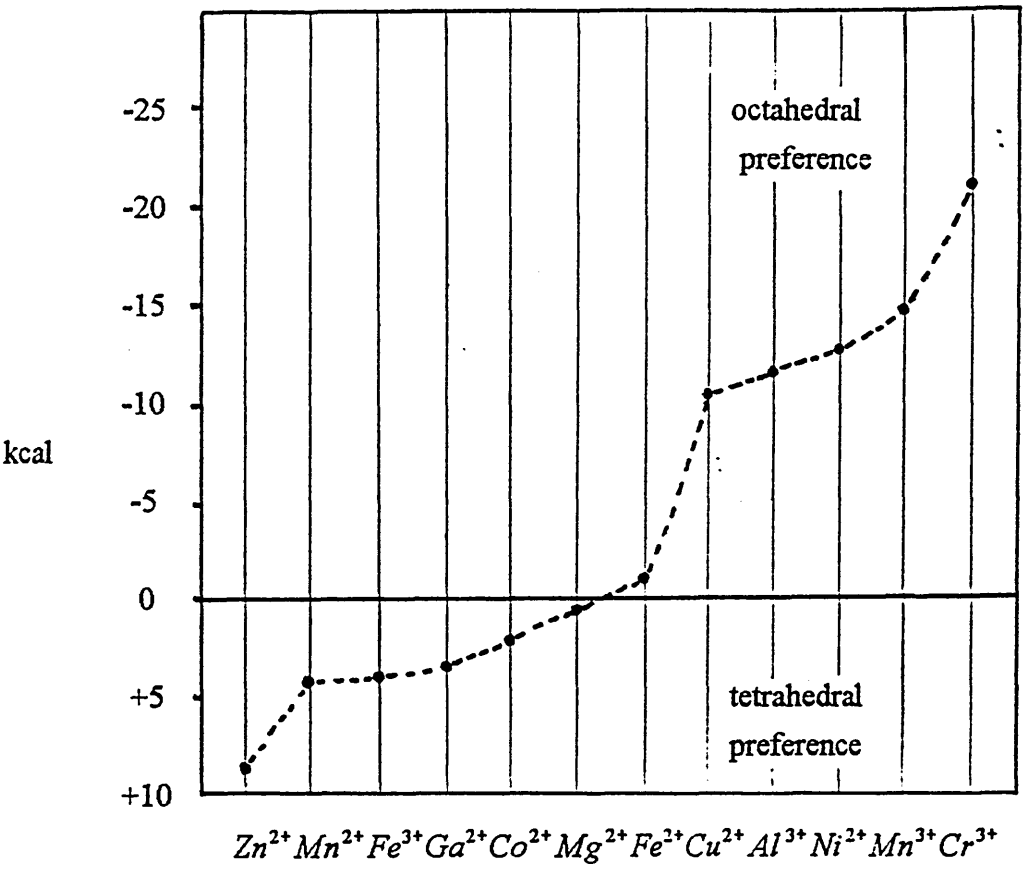

Figure 5.2 Emperical site preference energies for some divalent and trivalent ions in the spinel structure. (Navrotsky & Kleppa)

It can be seen from figure 5.2 that the ions commonly found in the spinel structure may be grouped roughly into three classes

(1) Those with large tetrahedral site preference; Zn^{2+}

(2) Those with small to zero tetrahedral site preference;
$Fe^{3+}, Ga^{3+}, Co^{2+}, Mn^{2+}, Mg^{2+}, Fe^{2+}$

(3) Those with large octahedral site preference;
$Cu^{2+}, Ni^{2+}, Al^{3+}, Mn^{3+}, Cr^{3+}$

Of significance to the structure of chromite is the large octahedral site preference of the Cr^{3+} ion and the small tetrahedral site preference of the Fe^{3+} ion . Although it has since been shown that the apparent site preference energy of an ion depends on the structure of the spinel into which it is substituted (O'Neill & Navrotsky 1983). The data determined by Navrotsky and Kleppa was obtained from synthetic spinels and in comparing the mineral spinel $MgAl_2O_4$ with synthetic $MgAl_2O_4$ it was found that natural spinel was completely normal and only exhibited a disordered structure when heated to 800°C This was attributed to a geological annealing process. Generally natural spinels are found to be normal spinels although the minerals magnesioferrite $MgFe_2O_4$ and the ulvöspinel $Ti(FeMg)_2O_4$, are thought to be disordered (Berry & Mason 1959).

Spinels can be readily identified by X-ray diffraction, differing only in the displacement of the lines due to the differeces in lattice size from one spinel to another.The lattice spacing of mixed spinels, such as chromite, varies proportionately to the content of the individual spinels present and can be calculated from the the molecular composition and the lattice spacing of the pure spinels (Vegard 1921). For inverse spinels the general diffraction pattern remains unchanged and the different types can therefore only be differentiated by precise line intensity measurements which show up the different effect of the ions as regards their scattering power. With most spinels it has not been possible to differentiate by this means as the scattering power is roughly the same.

5.2 MÖSSBAUER SPECTRA OF SIMPLE SPINELS

The tetrahedral site in the ideal spinel has cubic symmetry and therefore no electric field gradient at the cation, but the octahedral site has trigonal point symmetry giving an anticipated large electric field gradient. For a normal 2,3 spinel this would give rise to a

single line spectrum for compounds with ferrous ions in the tetrahedral (A) site and a quadrupole split spectrum for compounds with ferric ions in the octahedral (B) site. This was confirmed by work on the synthetic normal 2,3 spinels $ZnFe_2O_4$, $FeCr_2O_4$ (Mizoguchi & Tanaka 1963) and FeV_2O_4, $FeCr_2O_4$ (Rossiter 1965). An observed quadrupole splitting in the Mössbauer spectrum of $FeAl_2O_4$ reported by Rossiter and others (Ono, Ito & Syone 1966) was attributed to crystal imperfections causing a distortion in the electric field surrounding the tetrahedral site of the Fe^{2+} ion. Later work comparing the low temperature optical absorption spectra and the low temperature Mössbauer spectra of natural spinel and synthetic $FeAl_2O_4$ (Dickson & Smith 1976) suggested that the quadrupole splitting observed in $FeAl_2O_4$ was due to tetrahedral Fe^{2+} with some octahedral Fe^{2+}, indicating a degree of inversion of ~ 15%. The two doublets overlapping at room temperature but seperating at low temperature. This agreed with earlier observations on the optical absorption properties of $FeAl_2O_4$ (Slack 1964). The natural spinel $MgAl_2O_4$, with 2.4% Fe^{2+} as an impurity, had a room temperature spectra showing a single peak. This being assigned to Fe^{2+} in a near perfect tetrahedral site. The spectrum changed when the crystal was annealed to show quadrupole splitting similar to that of $FeAl_2O_4$. The quadrupole splitting in the annealed natural spinel was attributed to tetrahedral Fe^{2+}, with a changed atomic environment causing distortions in the electric field. The quadrupole splitting observed in annealed natural spinel agreed with earlier work (Ono, Chandler & Ito 1967) which found that the quadrupole splitting increased rapidly after the natural spinel crystal had been annealed above 1100°K. This would also to agree with the observations of Navrotsky and Kleppa in their thermodynamic treatment of cation distributions, which indicated that a natural spinel crystal would achieve a degree of inversion when heated to a temperature above 800°C.

The inverse synthetic spinels $FeNiAlO_4$ and $FeNiCrO_4$, with Fe^{3+} ions on the tetrahedral site, show a degree of quadrupole splitting (Mizoguchi & Tanaka 1963) which is ascribed to the heterogeneous nature of the B site occupation. The coexistence of divalent and trivalent ions giving rise to an electric field gradient on the A site. This next-nearest neighbour effect was investigated in the Mössbauer spectra of $Fe(Cr,Al)_2O_4$ spinels, where it was used to explain the increase in quadrupole splitting with the increase in the aluminium content of the spinel (Osborne, Fleet & Bancroft 1984).The effect of substitutions of ions on the A site on the Mössbauer spectra of Fe^{2+} ions on the A site by substituting Mg^{2+} and Zn^{2+} in the spinel $FeCr_2O_4$ showed that this second coordination sphere had minimal effect and no quadrupole interaction was observed (Osborne, Fleet & Bancroft 1983).

The inverse natural 4,2 spinel, the ulvöspinel Fe_2TiO_4, is thought to contain two kinds of Fe^{2+} ions, one located on the tetrahedral site and the other on the octahedral site. Its Mössbauer spectrum shows a broad doublet assigned to overlapping quadrupole splittings due to Fe^{2+} ion occupation of both A and B sites (Ono, Chandler & Ito 1968). The spectra at a range of temperatures between 4.2°K and 800°K failed to resolve any contributions from the two different sites and it was suggested that the temperature dependence of the splitting for the octahedral site is similar to that for the tetrahedral site. The normal 4,2 spinel $GeFe_2O_4$ with octahedral Fe^{2+}shows a large quadruploe splitting which is insensitive to temperature between 77°K and 300°K (Rossiter 1966). This result is similar to those obtained from experiments on octahedral Fe^{2+} ions in the normal 4,2 spinels $GeFe_2O_4$, $GeCo_2O_4$ and $GeNiO_4$ which showed large quadruploe splittings that were insensitive to temperature in the range 4·2°K to 300°K (Varret & Imbert 1974). This temperature insensitivity of the quadrupole splitting has also been observed for octahedral Fe^{3+} between the temperatures 26°C and 510°C in the synthetic spinel $ZnFe_2O_4$ (Mizoguchi & Tanaka 1963).

A 2,3 spinel, $FeGa_2O_4$, produced from a mixture of Fe, Fe_2O_4 and Ga_2O_3 in stochiometric proportions gave a room temperature spectrum on the first synthesis that cuold be interpreted as consisting of two quadrupole pairs. The outer pair, having isomer shift $\delta = 0.8 mms^{-1}$ and quadrupole splitting $\Delta = 2.9 mms^{-1}$, were compared to the lines attributed to octahedral Fe^{2+} in the spectrum of $GeFe_2O_4$. The inner pair had $\delta = 0.65 mms^{-1}$ and $\Delta = 1.2 mms^{-1}$, suggesting a comparison with results on $FeAl_2O_4$ attributed to tetrahedral Fe^{2+}. At 77°K the spectrum consists of two broad lines with $\delta = 0.9 mms^{-1}$ and $\Delta = 2.7 mms^{-1}$, which agreed with the previous experience of the author (Rossiter 1966) that the quarupole interaction at the octahedral site is insensitive to temperature but that at the tetrahedral site, when it occurs, shows a large temperature dependence. On further annealing, the compound gave a Mössbauer spectrum which showed that the outer peaks had decreased in intensity, leaving a predominant pair with $\delta = 0.6 mms^{-1}$ and $\Delta = 1.3 mms^{-1}$. At 77°K the spectrum showed a similar shape but with $\delta = 0.9 mms^{-1}$ and $\Delta = 2.3 mms^{-1}$ suggesting that most of the Fe^{2+} ions were on the tetrahedral site and that the structure was tending towards a normal spinel. In view of the complex geo-thermal conditions that natural spinels have experienced, this raises the possibility that spinels that are inverse when produced synthetically are normal in their natural state.

The results from the Mössbauer spectra of various simple spinels are summarised in table 5.1. These results have also been condensed into the following diagnostic generalisations: (Greenwood & Gibb 1971)

(1) chemical isomer shifts increase in the sequence δ (tetrahedral Fe^{3+}) < δ (octahedral Fe^{3+}) < δ (tetrahedral Fe^{2+}) < δ (octahedral Fe^{2+})

(2) quadrupole splitting for both Fe^{2+} and Fe^{3+} in sites of accurately cubic symmetry is zero; for non-cubic sites $\Delta(Fe^{3+}) \ll \Delta(Fe^{2+})$

Material	Phase	Temp.	Fe^{2+} A		Fe^{2+} B		Fe^{3+} A		Fe^{3+} B		Refer.
		°K	δ	Δ	δ	Δ	δ	Δ	δ	Δ	
			mms^{-1}		mms^{-1}		mms^{-1}		mms^{-1}		
$ZnFe_2O_4$	Normal	300							.36	.36	
		470							.27	.34	(1)
		630							.17	.34	
		783							.125	.34	
$FeNiAlO_4$	Inverse	514					.12	.50			(1)
		631					.17	.53			
$FeNiCrO_4$	Inverse	720					.14	.40			(1)
$FeCr_2O_4$	Normal	293	.94	0							(2)
FeV_2O_4	Normal	293	.91	0							(3)
$GeFe_2O_4$	Normal	77			1.0	2.9					(4)
		300			0.9	3.0					
$FeAl_2O_4$	Normal	77	1.3	2.8							(3)
		295	1.1	1.6							

All isomer shifts relative to metallic iron

References (1) Mizoguchi & Tanaka 1963

(2) Robbins et al 1971

(3) Rossiter 1965

(4) Rossiter 1966

Table 5.1 Mössbauer parameters for some spinels

The work of Rossiter on Fe_2GeO_4 and $FeGa_2O_4$, and Dickson and Smith on synthetic $FeAl_2O_4$, seem to favour the idea that the quadrupole splitting of octahedral Fe^{2+} is, in common with octahedral Fe^{3+}, temperature insensitive. Although Ono, Chandler and Ito state that in the case of Fe_2TiO_4, the temperature dependence of the splitting for the octahedral Fe^{2+} is quite similar to that for the tetrahedral Fe^{2+} and two different spectra for the two different sites could not be resolved.

As a precursor to the Mössbauer spectroscopy of chrome ores, it will be useful to consider a study of natural gahnite spinels (Waerenborgh et al 1990). Gahnite is a normal spinel with an ideal composition $ZnAl_2O_4$, but which in its natural form has minor concentrations of Fe and other elements (Mg, Cr, Mn etc.). These conditions mirror those experienced by the individual spinels of the chromite grains. The Mössbauer spectra of natural gahnite and their interpretation could act as a guide when interpretating the spectra of chromites. The spectra were fitted as a distribution of three doublets, one representing octahedral Fe^{3+} and two representing tetrahedral Fe^{2+}. The splitting of the octahedral component remained constant over the temperature range 77°K to 300°K, while those of the tetrahedral component showed a significant variation.

5.3 MÖSSBAUER SPECTROSCOPY OF CHROME ORES

The debate on attributing quadrupole splitting contributions to the various site combinations, encountered in the Mössbauer spectra of simple spinels, is mirrored in the controversy surrounding the fitting regime used to interpret the spectra of the chromite grains of chrome ores. Some investigators (Osborne, Fleet & Bancroft 1981) favour an ordered distribution of sites, with no evidence of tetrahedral Fe^{3+} or octahedral Fe^{2+}. The spectra being fitted as two broad doublets, corresponding to tetrahedral Fe^{2+} and octahedral Fe^{3+} with, generally, the tetrahedral contribution having

a larger value of isomer shift and quadrupole splitting. A refinment to this fitting schedule was suggested to explain the larger line width associated with the tètrahedral Fe^{2+} doublet (Zhe et al 1988). Arguing that the different cation combinations on the B sites give rise to different electric field gradients on the A sites and form a number of doublets with different quadrupole splitting. A room temperature Mössbauer spectrum of a chromite was fitted as one octahedral Fe^{3+} doublet and three tetrahedral Fe^{2-} doublets. Spectra taken at other temperatures showed that the quadrupole splittings assigned to the tetrahedral site varied with temperature, whilst that associated with the octahedral site showed no appreciable change.

Other research has favoured a disordered distribution of site occupation. In an investigation of chrome ores from different sites in Madagascar, U.S.S.R., Iran and South Africa, a complex fit of six or seven doublets was proposed with both tetrahedral Fe^{3+} and octahedral Fe^{2+} (Fatseas, Dormann & Blanchard 1976). A temperature dependent Fe^{3+}/Fe^{2+} population ratio due to a 'hopping effect' with different activation energies for the different materials being used to explain the disorder and the variation in the intensity of the doublets with temperature. The temperature dependence of the quadrupole splittings appeared to be small over the temperature range 100°K to 300°K, with only an octahedral Fe^{2+} site showing any significant variation. A disordered cation distribution and electron hopping has also been proposed in a study of Brazillian chromites (Da Silva et al 1980) and in a study of Indian chromites (Singh et al 1978). All these fitting models show a small quadrupole splitting contribution for tetrahedral Fe^{2+}.

Cuban chromites from the surface and different levels under the surface of the same ore formation show a variation in the Mössbauer spectra (Suarez, Garcia & Diaz 1990). The sample of one taken from far below the surface gave the complex spectrum nomally associated with chromite and was fitted as a disordered distribution. The sample taken

from the surface gave a single broad doublet similar to the spectrum of a chromite annealed in air at a temperature above 1000°C (Da Silva et al 1976)(Brooks et al 1987). This was fitted as two doublets, a tetrahedral Fe^{3+} and an octahedral Fe^{3+}.

5.4 REFERENCES

Bancroft G.M., Osborne M.D., Fleet M.E.

Solid State Communications, 47,623, 1983

Barth T.F.W., Posjnak E.

Journal of the Washinton Academy of Science, 21, 225, 1931

Berry L.G., Mason B.

'Mineralogy', W. H. Freeman, 1959, p.353

Brooks J.S., Smith R., Williams G.L.

Sheffield Hallam University Internal Report, 1987

Chataborky K.L.

Economic Geology, 60, 1660, 1965

Clark G.L., Ally A.

American Mineralogist, 17, 66, 1932

DaSilva E.G., Abras A., Sette Camara A.O.R.

Journal Physique Colloque, 37, C6-783 1976

DaSilva E.G., Abras A., Speziali N.L., Sette Camara A.O.R.

Applied Physics, 22, 389, 1980

DeWet J.F., Van Niekerk J.N.

Journal of Chemical Metallurgy, Min. Soc. South Africa, 53, 10, 1952

Dickson B.L., Smith G.

Canadian Mineralologist, 14, 206, 1976

Fatseas G.A., Dormann J.L., Blanchard H.

Journal of Physics, 12, 787, 1976

Greenwood N.N., Gibb T.C.

'Mössbauer Spectroscopy', Charman and Hall, 1971, p.259

Mizoguchi T., Tanaka M.

Journal of the Physics Society of Japan, 18, 1301, 1963

Navrotsky A., Kleppa O.J.

Journal of Inorganic Nuclear Chemistry, 29, 2701, 1967

Ono K., Ito A., Syono Y.

Physics Letters, 19, 620, 1966

Ono K., Chandler L., Ito A.

Physics Letters, 24(A), 273, 1967

Ono K., Chandler L., Ito A.

Journal of the Physics Society of Japan, 25, 174, 1968

Osborne M.D., Fleet M.E., Bancroft G.M.

Solid State Communications, 48, 663, 1983

Osborne M.D., Fleet M.E., Bancroft G.M.

Journal of Solid State Chemistry, 53, 174, 1984

Rait J.R.

'Third Report on Refractory Materials', The Iron and Steel Institute, Special Report No 32, 175, 1976

Rossiter M.J.

Journal of the Physical Chemistry of Solids, 26, 775, 1965

Rossiter M.J.

Physics Letters, 21, 128, 1966

Singh A.K., Jain B.K., Date S.K., Chandra K.

Journal of Applied Physics (D), 11, 769, 1978

Slack G.A.

Physics Review, 134, A1268, 1964

Suarez N., Garcia S., Diaz C.

Hyperfine Interactions, 57, 2295, 1990

Varret F., Imbert P.

Journal of the Physical Chemistry of Solids, 15, 215, 1974

Vegard L. (1921)

In Rait J.R., 'Basic Refractories', Iliffe, 1950, p. 195

Waerenborgh J.C., Annersten H., Erricson T., Figueiredo M.O., Cabral J.M.P.

European Journal of Minerals, 2, 267, 1990

Zhe L., Mingzhi J., Wei H., Milan L.

Hyperfine Interactions, 41, 819, 1988

CHAPTER SIX

MÖSSBAUER STUDIES OF CHROME ORES

6. MÖSSBAUER STUDIES OF CHROME ORES

Samples of chrome ores were kindly supplied by Steetley Refractories Limited. These were in powder form and several samples were prepared with a Mössbauer thickness $t \leq 1$ ($ 3.3). The spectra were originally recorded with a velocity range of ± 12 mms^{-1} to allow any magnetic hyperfine phases to be detected.

As all the samples supplied showed a similar Mössbauer spectrum with only paramagnetic phases, it was decided to conduct a detailed analysis of one ore sample, using a reduced velocity range of ± 4 mms^{-1}. The sample chosen was Masinloc 10, which is mined in the Phillipines and is the most common ore used by Steetley Refractories, at the present time, in the manufacture of chrome - magnesite bricks.

6.1 COLLECTION OF DATA

Initially two spectra of Masinloc 10 were recorded, one at room temperature and the other at 50°K. The lower temperature spectrum showed a greater range of quadrupole splitting that could be fitted relatively easily as two quadrupole doublets using MOSFITN (S 3.5) the parameters of which are shown in table 6.1. These two doublets were assigned to Fe^{2+} and Fe^{3+} by comparison with previously reported data (Table 6.1).

Temperature	δ	ΔE_Q	Γ	A%	χ^2
	mms^{-1}	mms^{-1}	mms^{-1}		
50°K	0.94	3.00	0.25	72	19.99
	0.33	0.61	0.21	28	

Table 6.1 Mössbauer parameters for RS057 (MOSFITN)

However it could be seen that the larger (Fe^{2+}) doublet had a very broad line width and also failed to fully describe the observed spectrum (Fig. 6.1). Dividing this broad quadrupole doublet into a distribution of two and then three smaller doublets gave a decrease in the χ^2 value ($ 3.5) from 19.9 to 6.6 and then to 3.2 respectively (Fig. 6.2) This four doublet model was then applied to the spectrum obtained at 300°K resulting in a χ^2 value of 1.8 (Fig. 6.3).

A variable temperature study of Masinloc 10 between 15°K and 600°K was performed and the spectra fitted using the model of one Fe^{3+} doublet and three Fe^{2+} doublets. Due to operating requirements and the limited availability of equipment some of the low temperature spectra were recorded under different operating conditions. The higher temperature spectra (325°K to 600°K) were recorded using the electric furnace. The lower temperature spectra were collected using the Displex system ($ 3.7).

The temperature dependence of the Mössbauer parameters thus obtained have been used to check the validity of the fitting model by comparing the data with those of other workers.

There are two independent methods for determining the Debye temperature θ_D and hence the recoil free fraction f_A of the absorber (Brooks, Williams & Allen 1991). The first method involves the accurate measurement of the changes in absorption line area with temperature whilst the second makes use of the second order Doppler shift of the resonance line which produces a small, but measurable, temperature dependent component to the chemical isomer shift. Both methods assume that the vibrational properties of the sample can be represented by the Debye model of solids.

The temperature dependence of the quadrupole splitting allows approximations to the distortions of the crystal field to be estimated.

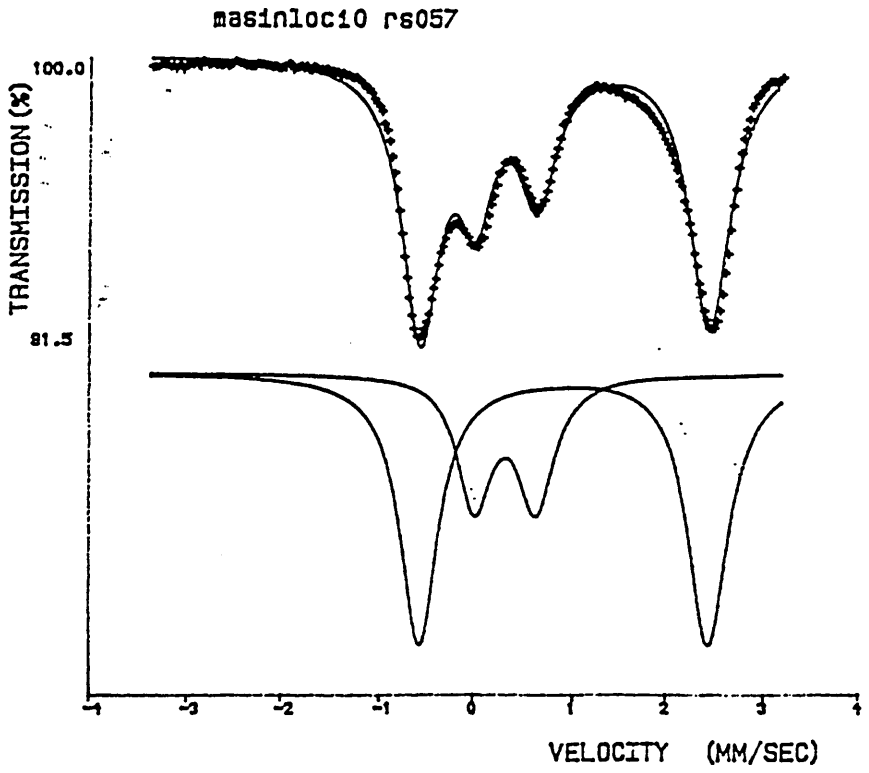

Figures 6.1 Two doublet for Masinloc 10 at 50°K

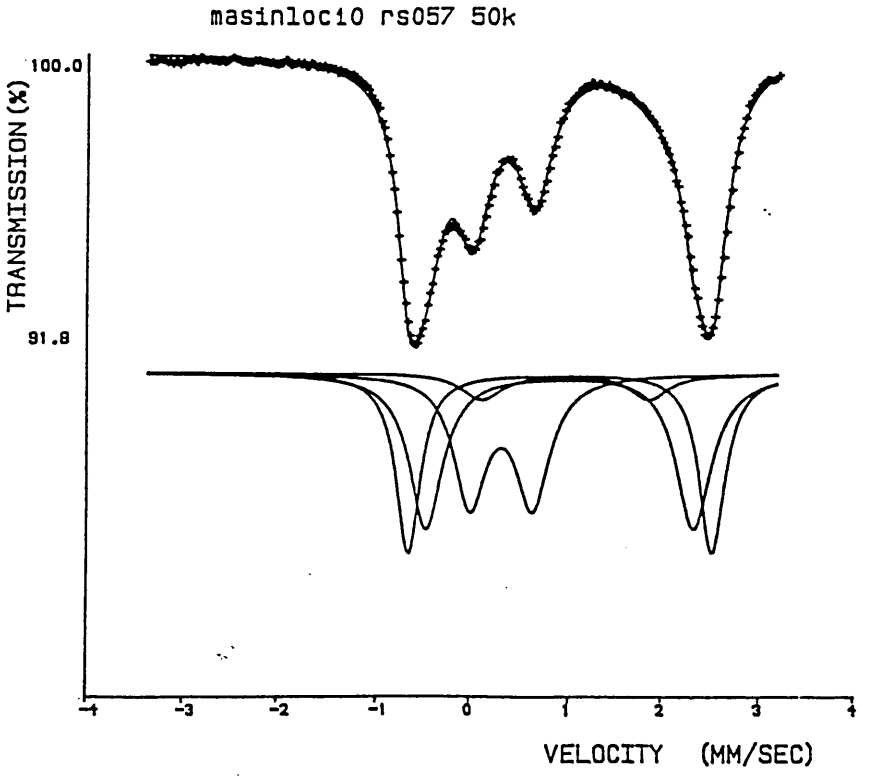

Figure 6.2 Four doublet fit for Masinloc 10 at 50°K

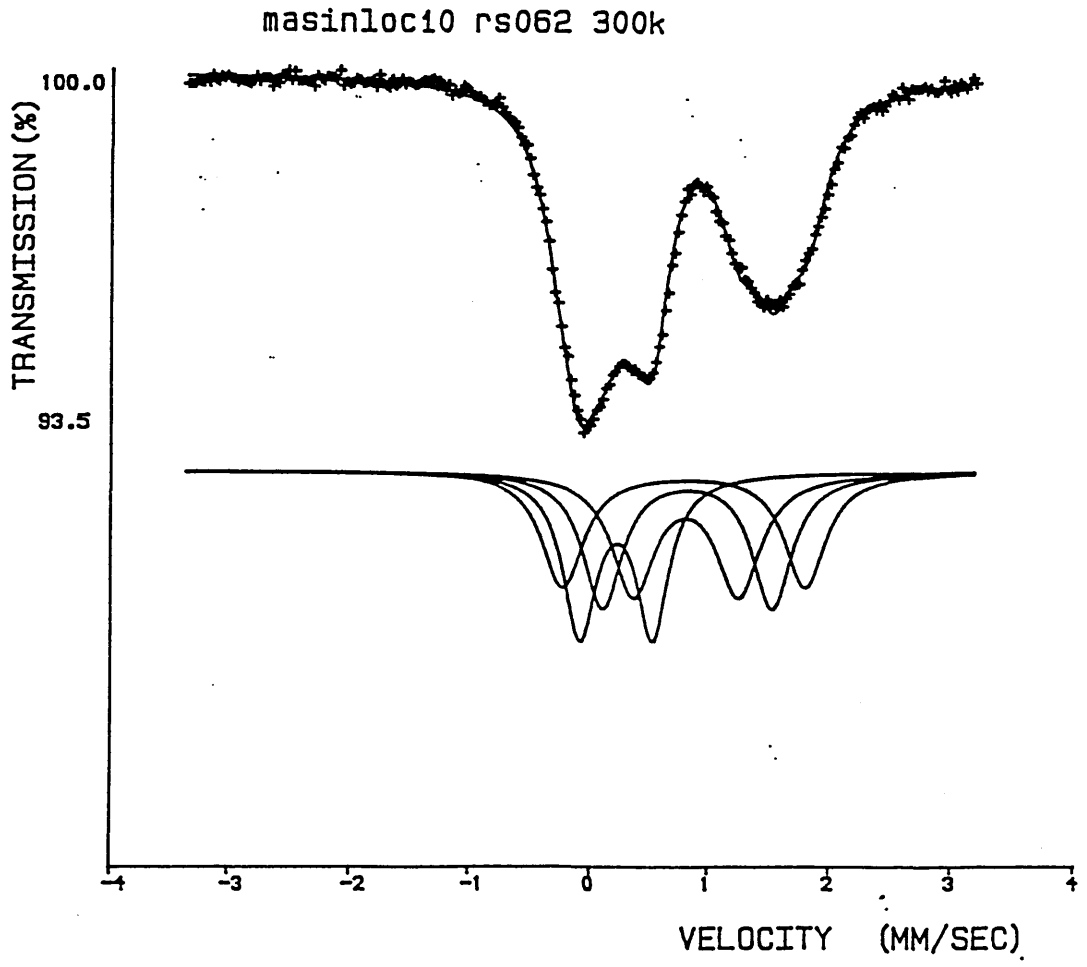

Figure 6.3 Four doublet fit for Masinloc 10 at 300°K

6.2 TEMPERATURE DEPENDENCE OF ABSORPTION AREA

For a monatomic cubic lattice, the Debye - Waller factor is given by (Boyle & Hall 1962)

$$2W = \frac{3E_0^2}{Mc^2 k_B \theta_D^2}\left[\frac{1}{4} + \left[\frac{T}{\theta_D}\right]^2 \int_0^{\theta_D/T} \frac{x}{e^x - 1} dx\right] \qquad (6.1)$$

M is the mass of the Mössbauer nucleus, k_B is the Boltzmann constant, c is the velocity of light and θ_D is the characteristic Debye temperature.

For thin Mössbauer absorbers (t < 1), the absorption line area A(T) is proportional to the recoilless fraction (Williams & Brooks 1975) and can be expressed as

$$A(T) = K\exp(-2W) = K\exp\frac{-3E_0^2}{Mc^2 k_B \theta_D^2}\left[\frac{1}{4} + \left[\frac{T}{\theta_D}\right]^2 D_1\left[\frac{\theta_D}{T}\right] - \right] \qquad (6.2)$$

where D_1 represents a Debye integral.

$$D_1(Z) = \int_0^Z \frac{x}{e^x - 1} dx \qquad (6.3)$$

D_1 has no exact analytical solution but high and low temperature approximations exist to within 0.1% error (Heberle 1971).

A variable temperature fitting program LNAT (S 3.5) uses a non-linear least square routine to obtain a best fit to equation 6.2 for a set of experimental data values of area and temperature.

As described previously, not all the spectra were recorded under the same conditions. The different source / detector geometry of the displex system and the furnace will lead to a different mean count rate and hence a different normalised absorption area. This problem can normally be overcome but in the case of the lower temperature spectra an additional difficulty arose. Because of pressure on the usage of the Mössbauer spectrometer at Sheffield Hallam University spectra were collected at different times over a period of two years introducing further variations. However, the higher temperature spectra (325°K to 600°K) were collected consecutively under the same experimental arrangements and this data was used in the LNAT program.

The variation of normalised area with temperature for the two proposed sites (Figs. 6.4 & 6.5) show a wide spread of data points. This is due to the spectra being broadened by the inhomogeneity of the material thereby introducing a variation in the fitting's parameters. The Mössbauer parameters obtained are given in table 6.2

Iron state	θ_D (°K)	f_{RT}
Fe^{2+}	350 - 400	0.72 - 0.77
Fe^{3+}	645 - 1494	0.90 - 0.97

Table 6.2 Debye temperatures and recoil free fractions for iron sites of Masinloc 10 (LNAT)

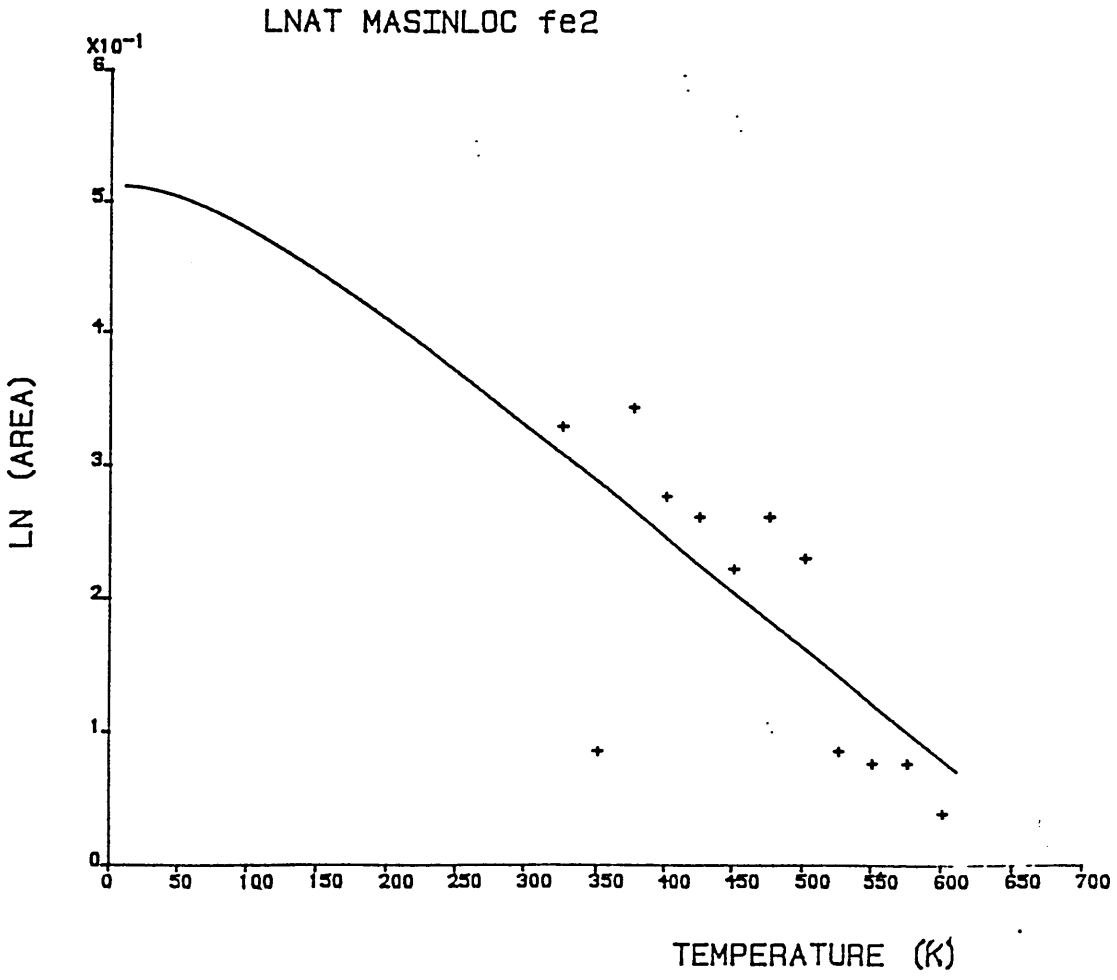

Figure 6.4 Normalised absorption area data for the Fe^{2+} site in Masinloc 10

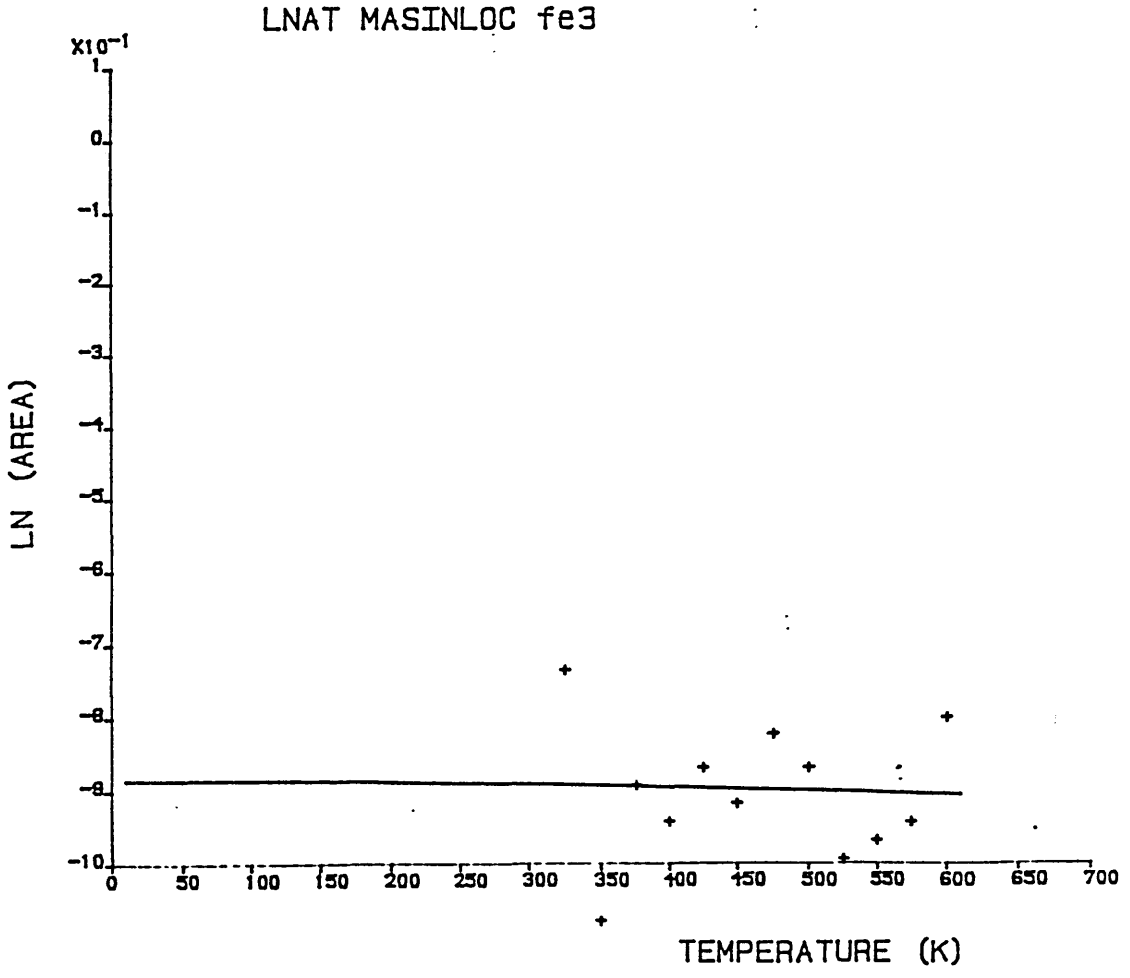

Figure 6.5 Normalised area data for the Fe^{3+} site in Masinloc 10

6.3 TEMPERATURE DEPENDENCE OF ISOMER SHIFT

In view of the difficulties encountered in collecting Mössbauer spectra more reliable results can be obtained from the temperature dependence δ(T) of the centre shift of the spectra as variations in the geometry and absorber thickness have no effect. The spectra were again fitted as three Fe^{2+} doublets and one Fe^{3+} doublet with the restriction that the three Fe^{2+} doublets in each spectrum have the same isomer shift.

The temperature dependence of the isomer shift δ can be written as

$$\delta(T) = \delta_{\text{int}} = \delta_{SODS} \tag{6.4}$$

in which δ_{int} is the intrinsic isomer shift

The second order Doppler shift δ_{SODS} results from the non-zero mean square velocity $\langle v^2 \rangle$ of the absorbing nuclei and can be expressed in terms of the Debye approximation (Pound & Rebka 1960) such that

$$\delta(T) = \delta_{\text{int}} - \frac{9}{2}\frac{k_B T}{Mc}\left(\frac{T}{\theta_D}\right)^3 \int_0^{\theta_D/T} \frac{x^3}{e^x - 1} dx \tag{6.5}$$

A computer fitting program ISODS (DeGrave et al 1984) fits a set of isomer shift data $\delta_{exp}(i)$ recorded at different temperature T(i) to an equation of the form of eqn. 6.5 to obtain the quantities θ_D and δ_{int}. Once θ_D is known, the f fraction at any temperature can be evaluated using the same method as in LNAT.

The variation of isomer shift with temperature for the two proposed sites in Masinloc 10 is shown in figures 6.6 & 6.7

Iron State	θ_D (°K)	f_{80}	f_{RT}
Fe^{2+}	385	0.90	0.75
Fe^{3+}	658	0.95	0.90

Table 6.3 Debye temperatures and recoil free fractions for iron sites of Masinloc 10 (ISODS)

6.4 TEMPERATURE DEPENDENCE OF QUADRUPOLE SPLITTING

The quadrupole splitting ΔE_Q of high spin Fe^{2+} has two contributions, one from the charge distribution of the aspherical 3d valence electron belonging to the $^5D_2$ $3d^6$ electron shell and the other from the charge distribution of the neighbouring ions in the crystal lattice. The temperature dependence of quadrupole splitting has been derived using crystal field theory and expressed in terms of a reduction factor F(T) (Ingalls 1964)

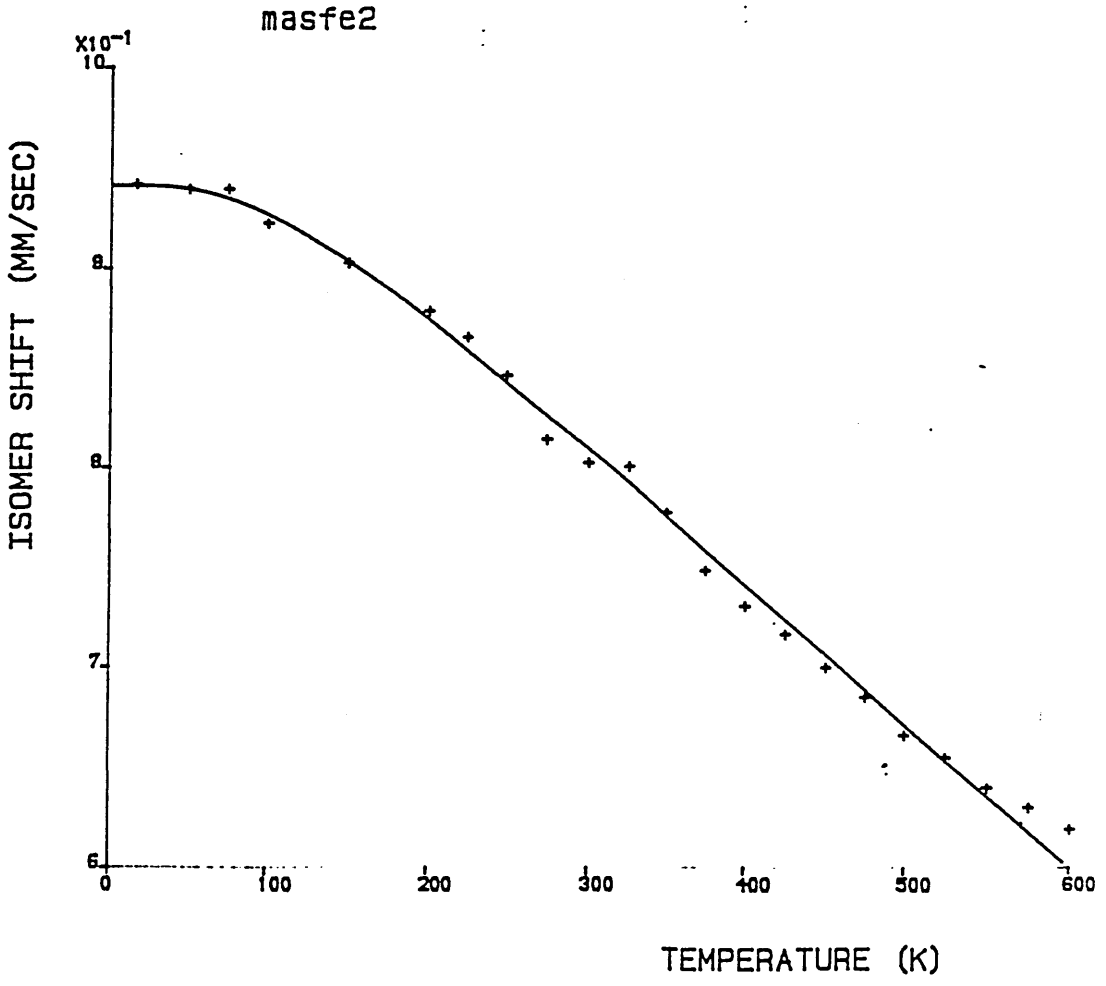

Figure 6.6 Temperature dependence of the Fe^{2+} isomer shift for Masinloc 10

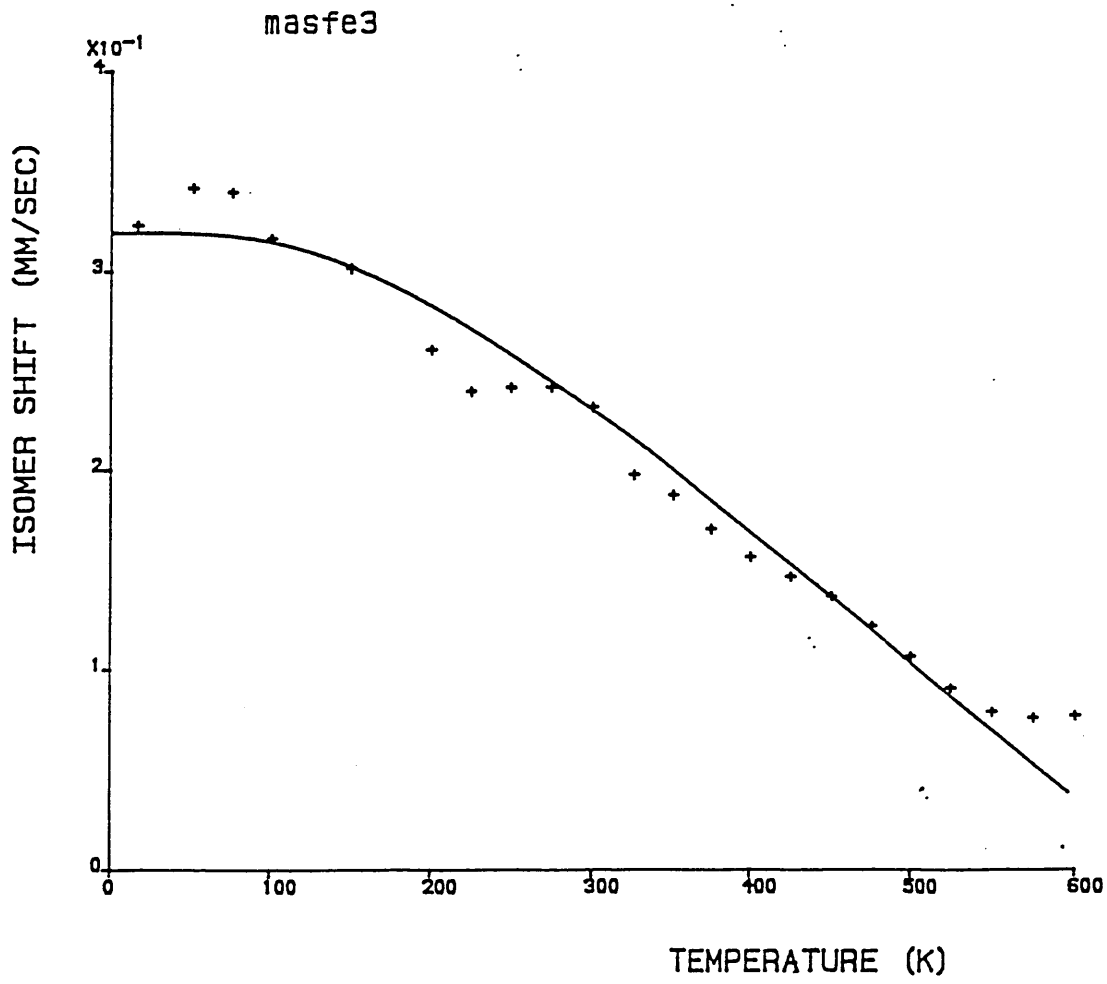

Figure 6.7 Temperature dependence of the Fe^{3+} isomer shift for Masinloc 10

$$\Delta E_Q(T) = \Delta E_{Q_{VAL}}(0)F(T) + \Delta E_{Q_{LAT}} \qquad (6.6)$$

where $\Delta E_{Q_{VAL}}(0)$ is the valence component of the quadrupole splitting a 0 Kelvin and $\Delta E_{Q_{LAT}}$ is the lattice component of the quadrupole splitting

The lattice contribution $\Delta E_{Q_{LAT}}$ for Fe^{2+} always acts in the opposite sense to $\Delta E_{Q_{VAL}}$ and reduces ΔE_Q from its maximum value. The effect of $\Delta E_{Q_{LAT}}$ is only of secondary importance to the quadrupole splitting.

The analysis assumes that there is a zero probability of thermal occupancy of the d_γ levels (Figure 6.8) because of the large energy difference, typically $10^4\ cm^{-1}$. Axial and rhombic distortions of the crystal field remove the degeneracy of the d_ε levels resulting in two excited states separated by energies Δ_1 and Δ_2 from the ground state. At all temperatures above absolute zero these excited states will be thermally occupied. If spin orbit coupling is neglected then F(T) can be expressed as (Ingalls 1964)

$$F(T) = \frac{\left[1 + e^{\frac{-2\Delta_1}{kT}} + e^{\frac{-2\Delta_2}{kT}} - e^{\frac{\Delta_1}{kT}} - e^{\frac{\Delta_2}{kT}} - e^{\frac{-(\Delta_1+\Delta_2)}{kT}}\right]^{\frac{1}{2}}}{1 + e^{\frac{\Delta_1}{kT}} + e^{\frac{-\Delta_2}{kT}}} \qquad (6.7)$$

where k is the Boltzmann constant

This describes the relationship appropriate to the crystalline field perturbation of an octahedral environment.

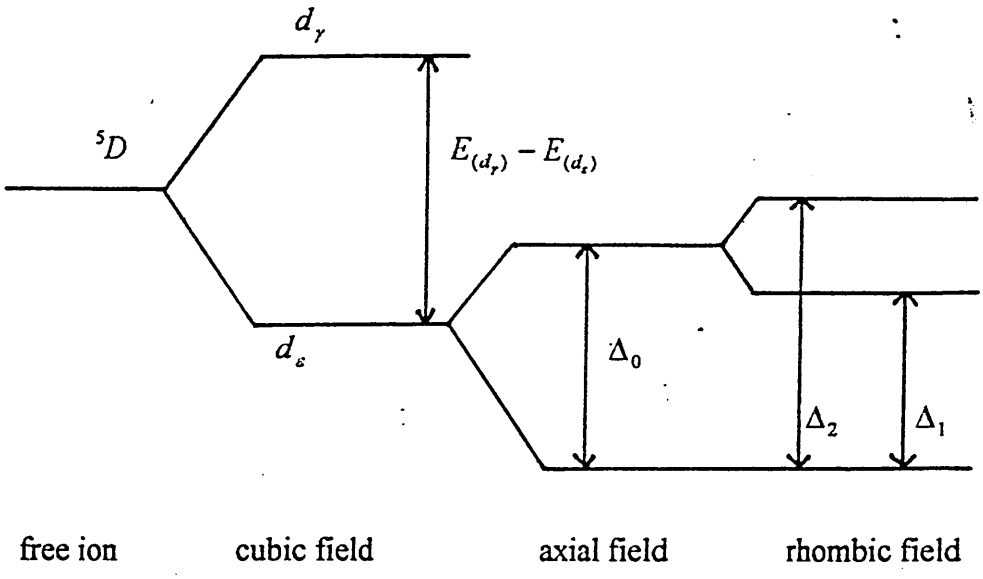

Figure 6.8 Energy level scheme for the Fe^{2+} ion under the action of the crystalline field

For a tetrahedral environment the formula has been recalculated to give the following relationship (Gibb & Greenwood 1965)

$$F = \frac{1 - e^{\frac{-\Delta_0}{kT}}}{1 + e^{\frac{-\Delta_0}{kT}}} \qquad (6.8)$$

where Δ_0 is the level splitting for an axial field

6.5 RESULTS

The Debye temperatures obtained from the analysis of the variation of isomer shift with temperature and, to a certain extent, the variations of normalised area with temperature

for the two proposed sites agree favourably with those obtained for some spinels from the temperature dependence of the isomer shift (DeGrave & Van Alboom 1991). These are shown in table 6.4.

Compound	q	C	$\theta_D(K)$	f_{80}	f_{RT}
(Mg,Cr) ferrite					
$MgCr_{0.5}Fe_{1.5}O_4$	+3	O_6, O_4 (1)	605	0.940	0.885
Spinel					
$Mg_{0.9}Fe_{0.1}Al_2O_4$	+2	O_4	340	0.875	0.697
Ilmenite					
$FeTiO_3$	+2	O_6	310	0.856	0.650
Ferrochromite					
$FeCr_2O_4$	+2	O_4	330	0.868	0.676

(1) Tetrahedral and octahedral components could not be resolved

Table 6.4 Characteristic Debye temperatures θ_D and recoil free fractions at 80°K and at room temperature, f_{80} and f_{RT}, for various compounds: q is the charge of the iron and C its co-ordination.

(DeGrave & Van Alboom)

It can be seen that the Debye temperature, and hence the recoil free fraction at room temperature (f_{RT}) and at 80°K (f_{80}) for Fe^{2+} in either site are similar. This corresponds to a study of a spinel (Fe_3O_4) and yttrium iron garnet (YIG) which showed that at room temperature the recoil free fraction for Fe^{2+} in the A site is 6% higher than for the B

site (Sawatzky et al 1969). This makes it very difficult to assign the quadrupole splittings of the Fe^{2+} contribution to any one site by determining the Debye tetmperature associated with the site. Clearly, some other method had to be used to determine which site the doublets were to be assigned.

The work of Ingalls (1964) on the temperature dependence of the quadrupole splitting has been investigated further by Gibb (1968). Using the crystal field approach the effect of the environment on the 3d shell was treated as a perturbation Hamiltonian

$$H = V_O + V_T + V_R + \lambda \hat{L} \cdot \hat{S} \qquad (6.9)$$

where V_O is the cubic field term, V_T is the tetragonal (or trigonal) term, V_R is the rhombic term and $\lambda \hat{L} \cdot \hat{S}$ is the spin orbit term.

The effect on the resulting 25 energy levels was computed as a 25x25 matrix. The parameters pertinent to eqn. 6.9 being

D_q - the cubic field parameter

D_s - the axial field parameter

D_r - the rhombic field parameter

λ - the spin-orbit coupling parameter

A series of graphs of the variation of reduction factor F with temperature for several parameter conditions were drawn. A theoretical curve was also fitted to data obtained by Ono, Ito & Syono (1966) on $FeAl_2O_4$ which showed that the environment of the Fe^{2+} ion corresponds to that for the tetrahedral (A) site. The parameters calculated were

$$D_Q = -1000cm^{-1}$$
$$D_S = -56.8cm^{-1}$$
$$D_R = 0$$
$$\lambda = -80cm^{-1}$$

The reduction factor temperature dependence curves for octahedral Fe^{2+} are generally flatter, corresponding to experimental data obtained for Fe^{2+} ions in the octahedral site of some 4,2 spinels (Varret & Imbert 1974). But, in the absence of a rhombic field, i.e. $D_R = 0$, the curve above approximately 150°K closely resembles that of the tetrahedral environment. However, below 150°K the reduction factor decreases (figure 6.9).

In their study of the ulvöspinel Fe_2TiO_4, Ono, Chandler and Ito (1968) produced a theoretical curve, also based on the work of Ingalls, for the temperature dependence of the quadrupole splitting for the compound on the premise that it was an inverse spinel. The curve, which is reproduced in figure 6.10, shows a reduction in the quadrupole splitting towards 0°K. However, because magnetic hyperfine structures were observed below 140°K the authors were not able to provide quadrupole splitting data below this temperature.

The variation of the weighted average of the quadrupole splittings with temperature for Masinloc 10 is shown in figure 6.11. The shape of the curve can clearly be seen to resemble the theoretical curve for a tetrahedral environment and it would appear that the proposed fitting model is correct, with no evidence of inversion in the spinel structure.

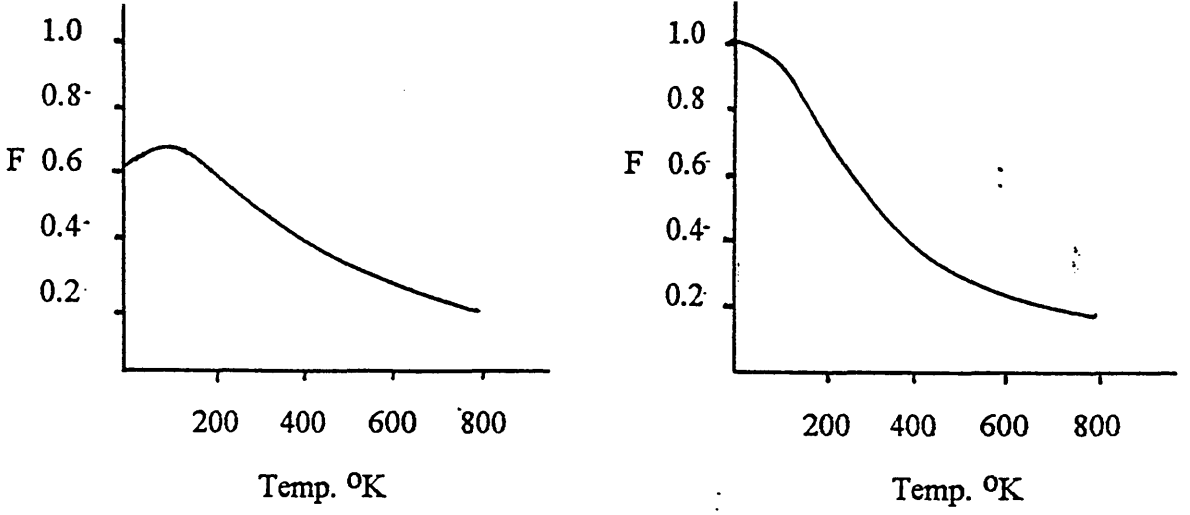

(a) Calculated reduction factor values for octahedral Fe^{2+} with

$D_Q = 1000cm^{-1}, D_S = -1000cm^{-1}$

$D_R = 0, \lambda = -80cm^{-1}$

(b) Calculated reduction factor values for tetrahedral Fe^{2+} with

$D_Q = -1000cm^{-1}, D_S = -50cm^{-1}$

$D_R = 0, \lambda = -80cm^{-1}$

Figure 6.9 (Gibb 1968)

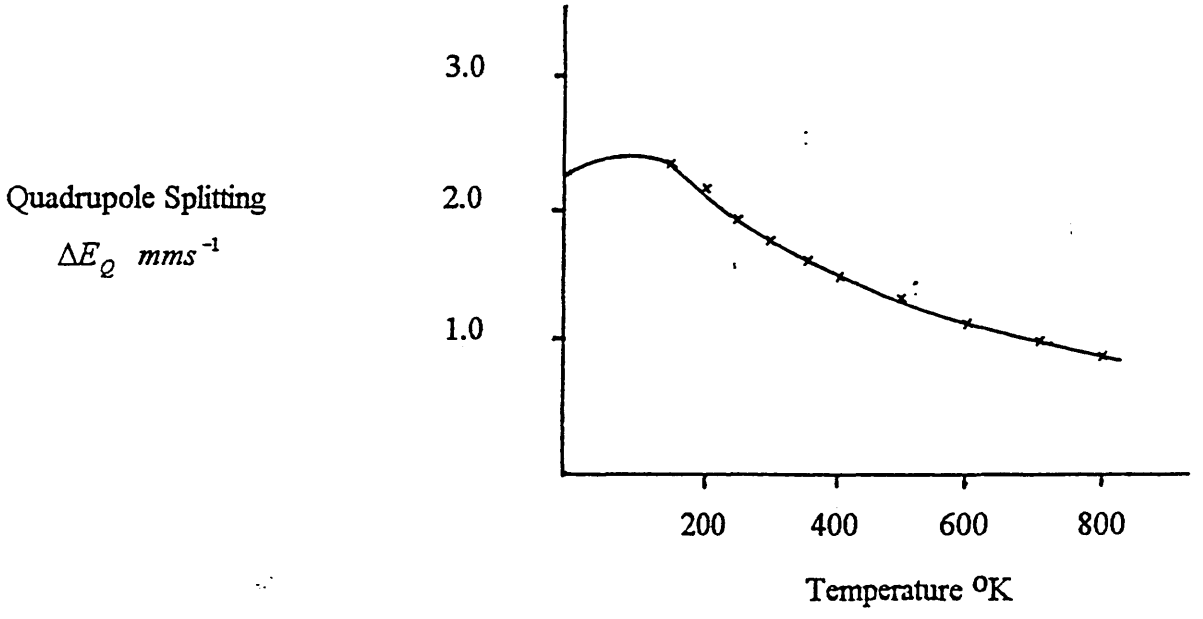

Figure 6.10 Variation of ΔE_Q with temperature for Fe_2TiO_4. Theoretical curve and experimental data (Dao, Chandler & Ito)

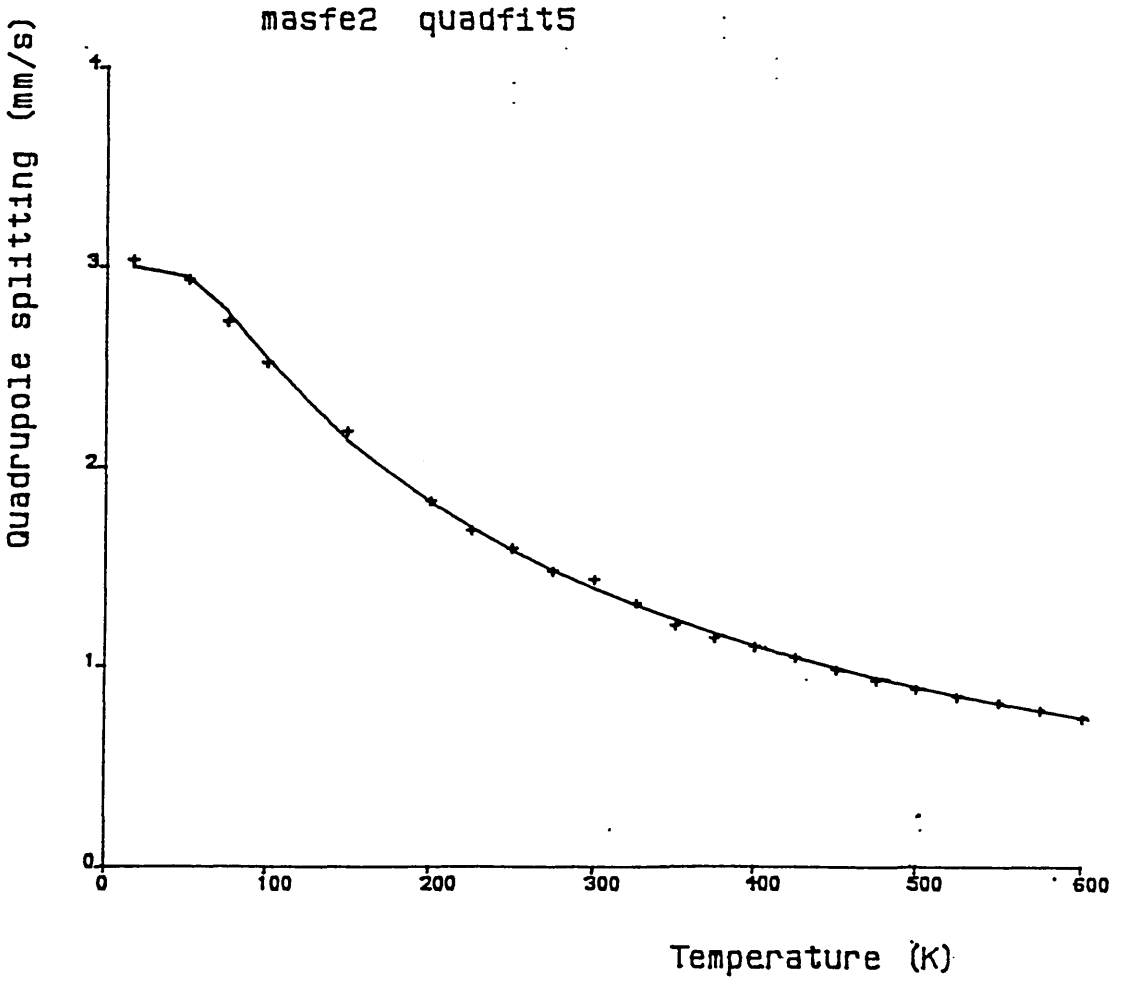

Figure 6.11 Temperature dependence of the Fe^{2+} quadrupole splitting for Masinloc 10

6.6 Fe^{2+} / Fe^{3+} RATIOS FOR SOME CHROME ORES

Using the parameters obtained, the Fe^{2+} / Fe^{3+} ratios were calculated for some chrome ores. These were compared to estimations of the molecular compositions chrome ores based upon average lattice spacings and average chemical analysis (Rait 1950). The fits, using the proposed model, of Turkish chrome and Cuban chrome at 80°K and room temperature (figures 6.12 & 6.13) were used in the calculation of the Fe^{2+} / Fe^{3+} ratio. These are shown in table 6.5

Chrome Ore	Fe^{2+} / Fe^{3+} Ratio (1)	Fe^{2+} / Fe^{3+} Ratio (2)
Cuban	1.6	4.4
Turkish	2.3 - 3.0	1.5
Masinloc 10	2.6 - 3.6	–

(1) This work

(2) Rait (1950)

Table 6.5 Fe^{2+} / Fe^{3+} Ratios

It can be seen that the results obtained bear little similarity to those proposed by Rait. However, Rait pointed out that the calculations were intended to arrive at an estimation of the composition, by using Vegard's law (\$ 5.1) to calculate the lattice spacing for the ore concerned, thus showing that the spinels were balanced, i.e. an equal number of AO and B_2O_3 phases, and not an attempt at calculating the Fe^{2+} / Fe^{3+} ratio.

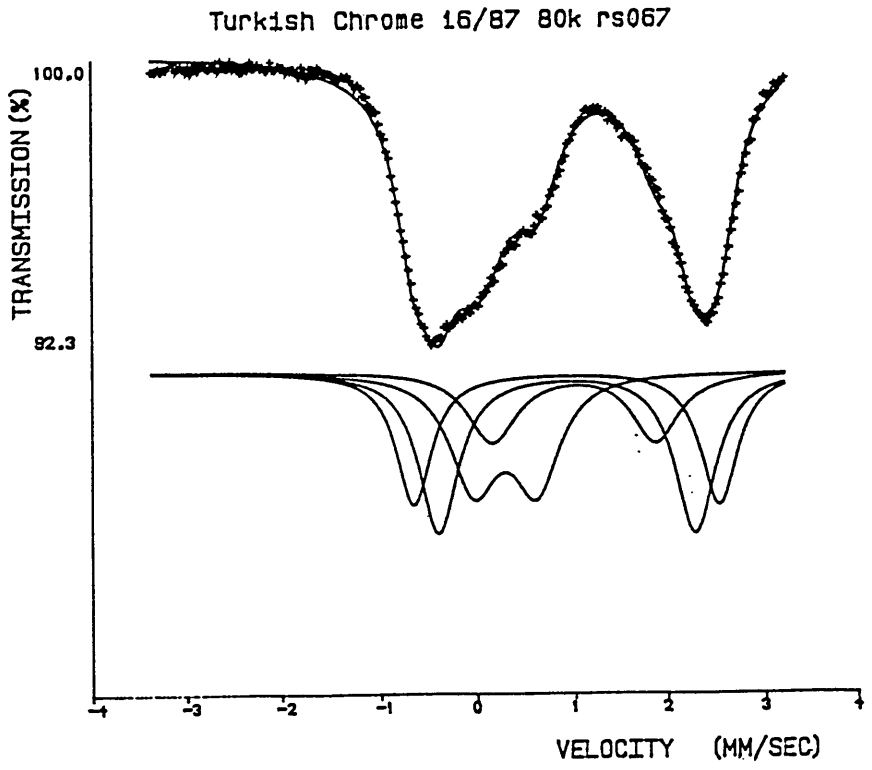

(a)

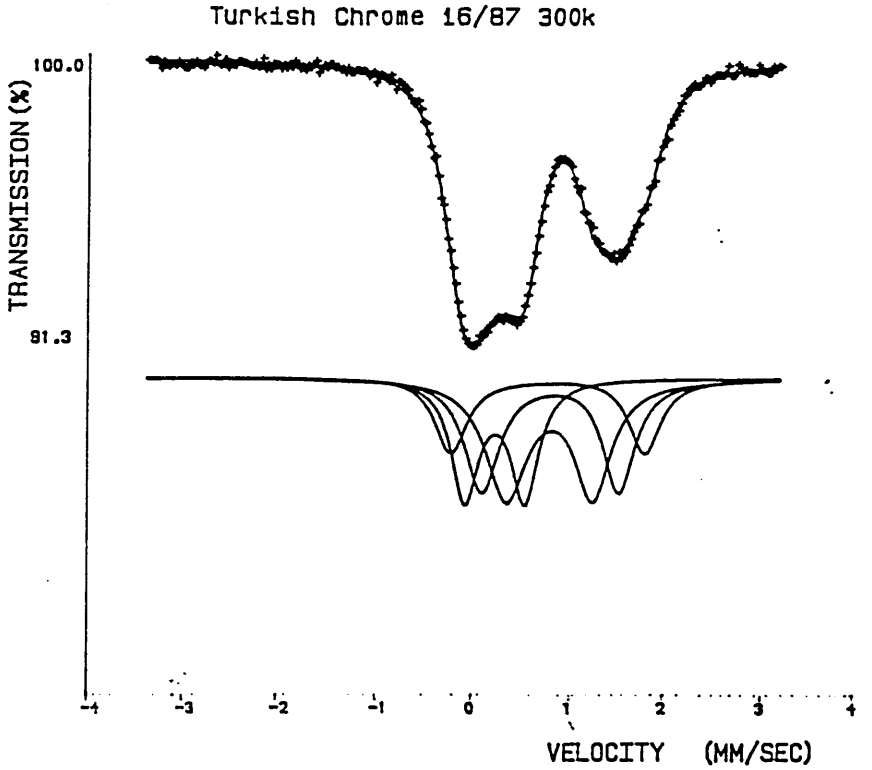

(b)

Figure 6.12 Four doublet fit for Turkish chrome at 80°K (a) 300°K (b)

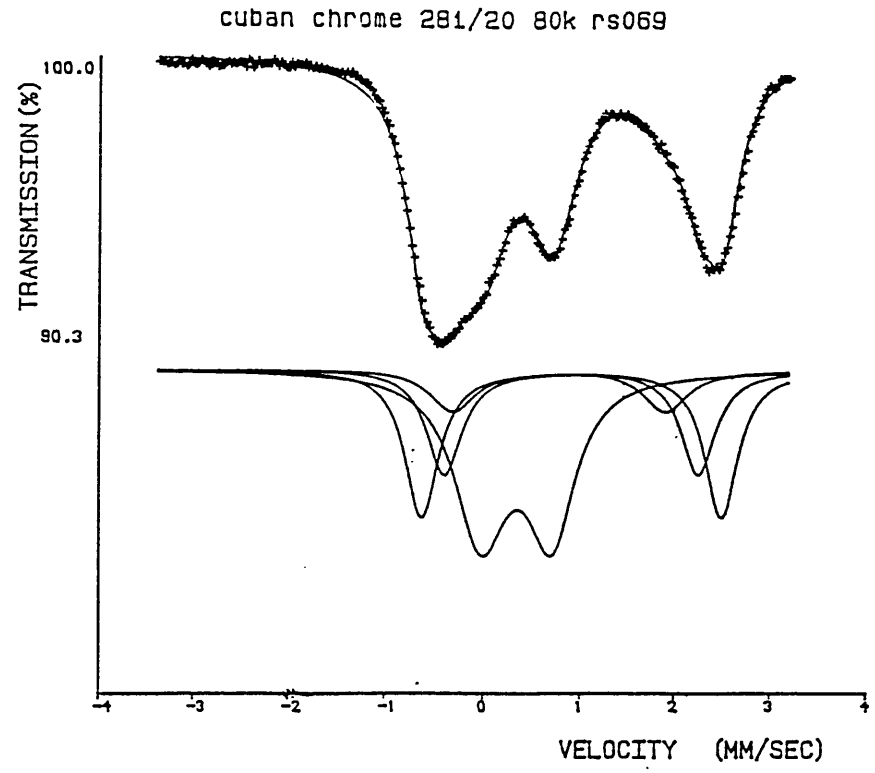

(a)

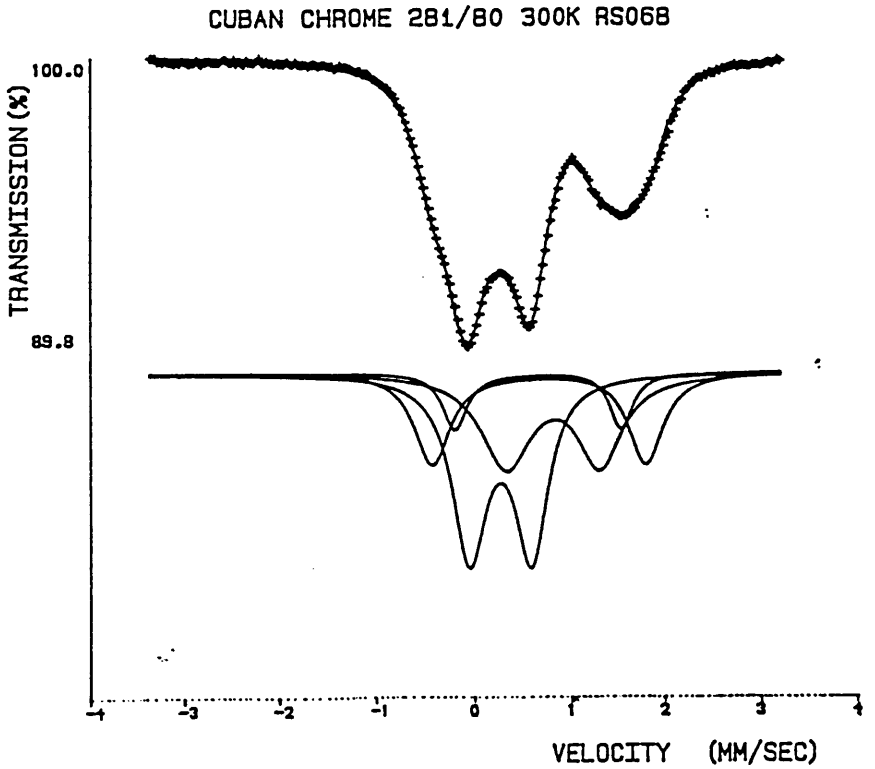

(b)

Figure 6.13 Four doublet fit for Cuban chrome at 80°K (a) 300°K (b)

An attempt was made to estimate the Fe^{2+} / Fe^{3+} ratio of chrome ores using the Mössbauer effect by Fatseas et al (1976) using a fitting model of six or seven doublets, that allowed for Fe^{2+} and Fe^{3+} ions on both A and B sites. The main conclusion drawn from this work was that electron hopping was evidenced by a reduction in the Fe^{2+} / Fe^{3+} ratio with increase in temperature. However, this conclusion did not take into account the differing recoil free fractions associated with the different ion states.

The variation of quadrupole splitting with temperature for tetrahedral Fe^{2+} (figure 6.14) showed little variation over the temperature range 50°K to 300°K, contrary to the findings of other workers (Ono, Ito & Syono 1966; Ono, Chandler & Ito 1968) and the theoretical model proposed by Gibb (1968).

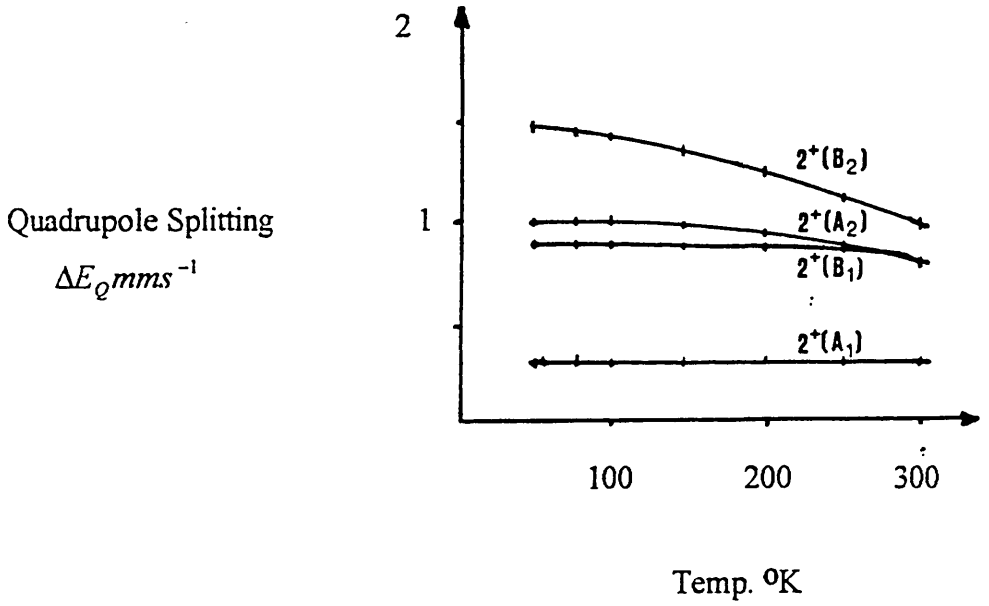

Figure 6.14 Temperature dependence of Fe^{2+} quadrupole splitting for Madagascan chrome, A and B sites.

(Fatseas et al)

6.7 DISCUSSION

From assessments of drive linearity it is usual to quote errors of ± 0.01 mms^{-1} for the isomer shift and line width and 0.02 mms^{-1} for the quadrupole splitting of 'thin' crystalline materials recorded over a range of ± 4 mms^{-1}. However, the heterogeneous nature of the materials investigated led to a departure of the absorption lines from a Lorenztian shape and an uncertainty in assigning values to the ferrous and ferric ion parameters leading to larger error values. Other works on similar materials (Williams 1990) has specified error values of ± 0.02 mms^{-1} for the isomer shift and line width and ± 0.04 mms^{-1} for the quadrupole splitting and these values have been adopted for all the spectra. The error on absorption area is somewhat larger and in order to learn more about the distribution of iron sites within the chromites future work could include the fitting of the spectra using the quadrupole splitting distribution program PQH (S 3.5).

All the chrome ores examined, seven in total, showed similar Mössbauer spectra, which could be fitted as one Fe^{3+} doublet with octahedral co-ordination and three Fe^{2+} doublets with tetrahedral co-ordination, suggesting a normal spinel structure, with no evidence of inversion or electron hopping.

A natural extension to this work would be a study of the processes involved in the firing of the chrome ore and magnesite mix in the manufacture of chrome magnesite bricks.

6.8 REFERENCES

Boyle A.J.F., Hall H.E.

Reports on Progress in Physics, 25, 441, 1962

Brooks J.S., Williams G.L., Allen D.W.

Physics and Chemistry of Glasses, 35(5), 171, 1992

DeGrave E.,Vanleerberghe R., Verdonck L., DeGeyter G.

Phsics and Chemistry of Minerals, 11, 85, 1984

DeGrave E., Van Alboom A.

Physics and Chemistry of Minerals, 18, 337, 1991

Gibb T.C., Greenwood N.N.

Journal of the Chemical Society, 6989, 1965

Gibb T.C.

Journal of the Chemical Society (A), 1439, 1968

Heberle J.

Mössbauer Effect Methodology, 7, 299, 1971

Ingalls R.

Physical Review, 133(3A), A787, 1964

Ono K., Ito A., Syono Y.

Physics Letters, 19(8), 620, 1966

Ono K., Chandler L., Ito A.

Journal of the Physics Society of Japan, 25(1), 174, 1968

Pound R.V., Rebka G.A.

Physical Review Letters, 4, 274, 1960

Rait J.R.

'Basic Refractories', Iliffe,1950 p.204

Sawatzky G.A., Van der WoudeF., Morrish A.H.

Physical Review, 183(2), 383, 1969

Varret F., Imbert P.

Journal of the Physics and Chemistry of Solids, 15, 215, 1974

Williams J.M., Brooke J.S.

Nuclear Instrumentation Methods, 128, 363, 1975

Williams G.L.

'Using MOSBAR under VM/CMS', Sheffield Hallam University Computer Services V6/3.56, 1988

Williams G.L.

Ph. D. Thesis, Sheffield Hallam University, 1990, p.126

ACKNOWLEDGEMENTS

There are a number of people who have been very patient and helpful during the time that I worked on the project that culminated in the writing of this thesis and to whom sincere thanks and gratitude are due. Foremost on the list is Professor John Brooks, who fulfilled admirably the role of supervisor by having faith in me and finding time in his busy schedule to offer encouragement and advice. I am also indebted to Dr. Sue Forder for her help in clarifying several aspects of Mössbauer spectroscopy. My thanks are also due to Dr. Gavin Williams for explaining the programs in the Mössbauer suite on the Apollo 570 and for guiding me through them on several occasions. A special mention should be made of Mr. Brian Didsbury of the School of Engineering workshops for the skill enthusiasm he displayed in constructing the Mössbauer furnace. Finally, I would like to thank all my colleagues in the School of Science for their help over the years, especially Kevin Blake for allowing me to use his computer to type the thesis and Terry Gaunt for showing me where my future lay.

COURSES AND CONFERENCES ATTENDED

Courses:

Spring 1989 'Introduction to Mössbauer Spectroscopy'

10 x 1 hour session, S.H.U.

Conferences:

R.S.C. Mössbauer Discussion Group Meetings:

July 1988	Manchester University
July 1991	City University
Sept. 1992	Nottingham University
Sept. 1993	Nottingham University